Physics – Uspekhi **67** (6) 533 – 560 (2024)

REVIEWS OF TOPICAL PROBLEMS PACS numbers: 52.27.Lw, **96.12. – a**, **96.20. – n**

Physical processes of formation and features of the plasma–dust exosphere of the Moon

L M Zelenyi, A V Zakharov, S I Popel, I A Kuznetsov, E V Rosenfeld

DOI: https://doi.org/10.3367/UFNe.2023.09.039567

Contents

Abstract. We review studies of physical processes associated with the impact of external factors in outer space — flows of micrometeoroids and solar radiation — on the lunar regolith. Under the influence of these factors, regolith microparticles can detach from the surface and levitate. Near-surface plasma and levitating dust particles form a plasma–dust exosphere of the Moon. Under anthropogenic effects on the lunar environment, charged levitating microparticles can have an extremely negative impact on the engineering systems of lunar landers and on the activity and health of astronauts on the Moon. Based on information gained by automated and manned lunar missions and in laboratory experiments, we discuss modern ideas about physical processes occurring near the Moon's surface. Unsolved problems associated with the plasma–dust exosphere of the Moon are considered, and the principal strategies for their solution are outlined.

Keywords: Moon, plasma, lunar dust, solar wind, micrometeoroids, regolith, exosphere

L M Zelenyi [1, a], **A V Zakharov** [1, b], **S I Popel** [1, 2, c], **I A Kuznetsov** [1, d], **E V Rosenfeld** [3, e]
[1] Space Research Institute, Russian Academy of Sciences, ul. Profsoyuznaya 84/32, 117997 Moscow, Russian Federation
[2] HSE University, ul. Myasnitskaya 20, 101000 Moscow, Russian Federation
[3] Mikheev Institute of Metal Physics, Ural Branch of the Russian Academy of Sciences, ul. S. Kovalevskoi 18, 620108 Ekaterinburg, Russian Federation
E-mail: [a] lzelenyi@cosmos.ru, [b] zakharov@cosmos.ru, [c] popel@iki.rssi.ru, [d] kia@cosmos.ru, [e] evrosenfeld@gmail.com

Received 17 July 2023, revised 18 September 2023
Uspekhi Fizicheskikh Nauk **194** (6) 569 – 599 (2024)
Translated by S Alekseev

1. Introduction

The Moon was the first extraterrestrial body to attract the attention of space exploration pioneers. In the 1960s and early 1970s, a series of Soviet and American automated landers and six crewed NASA Apollo missions conducted a lunar exploration program unprecedented in both intensity and scope. As a result of a large number of experiments, unique breakthrough data on the material of the lunar surface and its plasma environment were obtained. The robotic and crewed expeditions returned more than 300 kg of samples of lunar material to Earth for laboratory studies. The use of lunar rovers and direct human activity on the surface of the Moon played the role, as it were, of active experiments that allowed gaining profound experience in studying the natural environment of the Moon.

One of the least expected results of these studies was the discovery of a glow above the surface of the Moon (a celestial body that lacks an atmosphere) in the terminator region [1, 2]. This glow was recorded by several television cameras installed on Russian and American robotic landing vehicles and by astronauts orbiting the Moon in crewed spacecraft. Interpreting the lunar horizon glow (LHG) led to the conclusion that sunlight is scattered by lunar dust microparticles that levitate above the surface. At first glance, a noticeable amount of dust above the surface of a celestial body lacking an atmosphere would suggest either high meteorite activity or intense volcanic activity on the Moon. However, the LEAM (Lunar Ejecta and Meteorites) experiment [3] showed that very rarefied, but still noticeable, dust clouds arise above the surface of the Moon in the terminator region. The appearance of dust particles over the surface of the Moon cannot be explained by weak seismic vibrations caused by tidal forces due to the eccentricity of the Moon's orbit and/or continuous impacts of micrometeorites [4–6]. It was therefore assumed

that the most likely cause of the lift force in this case is Coulomb interaction.

Over the past decades, theoretical (see, e.g., [7–12]) and laboratory (see, e.g., [13, 14]) studies have been carried out aimed at experimentally modeling the physical processes that give rise to dust particles above the surface of the Moon. It turned out that this phenomenon is associated with a combined effect of external factors acting on the lunar surface: flows of micrometeorites and solar radiation. These external factors have been acting constantly during previous geological epochs and are currently active on the surface of the Moon, lacking an atmosphere, and cause fine-graining and, to a degree, chemical transformations of the lunar soil. As a result, regolith is formed, a significant part of which consists of particles of micron and submicron sizes, called lunar dust. The dominant role here is played by impact processes during bombardment with high-speed micrometeoroids. Because regolith is a good insulator [15, 16], exposure to ultraviolet (UV) radiation from the Sun and plasma flows of the solar wind induce a positive electric charge of the regolith on the illuminated surface (when the Sun is quiet); a cloud of photoelectrons then forms above it, creating a near-surface electric field and the so-called double plasma sheet. The Coulomb forces F_e in the electric field of this sheet act on the microparticles of lunar dust, overcoming the van der Waals adhesion forces F_a and the gravitational force F_g acting on the particles, allowing the lofting of particles, i.e., their detachment from the surface of the regolith. At $F_e \sim F_g$, dust particles can levitate above the surface of the Moon, forming a near-surface plasma–dust environment — the lunar exosphere. Sunlight scattered by particles suspended above the surface creates a glow that can be observed under certain conditions. However, the mechanism of the appearance of electrostatic forces capable of taking a microparticle off the regolith surface remains controversial [6].

During the Apollo crewed missions, American astronauts reported that levitating charged dust particles could be extremely aggressive. By affecting sensitive elements of service systems and scientific equipment of the landing vehicles, for example, thermal radiators, solar panel elements, and optical surfaces, such particles can disrupt their nominal operation and even lead to malfunction. In addition, American astronauts reported that lunar dust can penetrate through air-proof seals and negatively affect the work of astronauts on the surface of the Moon, reaching into the lungs and onto the human body, causing irritation of the skin and eyes [17]. This property of lunar dust microparticles is sometimes called toxicity (see, e.g., [18]).

Analyses of observations of glow over the lunar surface, the results of measurements of the regolith surface potential, and theoretical studies and laboratory modeling have brought about advances in understanding the dynamics of plasma–dust processes on the Moon. However, many unresolved problems remain.

Briefly, conditions near the surface of the Moon can be characterized as follows:

— a low surface gravity (1.622 m s^{-2}, approximately 1/6 of Earth's);

— a deep vacuum (approximately 10 nPa); the concentration of particles near the surface of the Moon is 15 orders of magnitude less than on Earth;

— regolith exposed to flows of intense electromagnetic radiation from the Sun, solar wind plasma, and high-energy charged particles (the penetrating radiation level on the Moon is 200–1000 times higher than on Earth);

— depending on the relief, a sharp boundary between light and shadow on the surface of the regolith (penumbra is nearly absent);

— the angle of inclination of the Moon's rotation axis to the ecliptic plane (88.5°) results in the presence of completely shadowed and constantly illuminated areas in the polar regions;

— deep changes in daily temperature, up to 300 K ($\sim$ 400 K during the day and $\sim$ 100 K during the night);

— charged dust particles present above the regolith surface whose characteristic size ranges from tens of nanometers to hundreds of micrometers;

— under the influence of UV radiation and solar wind plasma flows, a positive electric potential of several volts is formed on the surface of the Moon on the illuminated side, and a negative potential, up to hundreds of volts, on the shadowed side; when the Moon crosses the geomagnetic tail, the potential on the night side can reach several kilovolts;

— lunar dust, formed during the destruction of bedrock in collisions with high-speed micrometeoroids, is made of fine-grained microparticles of irregular shape with sharp edges (similar to crushed glass), with the mean size (determined by mass assuming their sphericity) is tens of micrometers;

— the terminator region and surface inhomogeneities with sharp boundaries of light and shadow are special as regards the surface potential distribution and near-surface electric fields.

In recent years, the space agencies of the Space Club countries have been planning the resumption of research and possible subsequent exploration of the Moon. In this regard, interest in more profound studies of the physical processes due to the dynamics of lunar dust and their impact on landers and their engineering systems is growing significantly. There is a need to develop technologies to reduce the negative impact of lunar dust on landing vehicles and on the activities and health of astronauts.

In this review, we analyze the physical processes associated with the formation and dynamics of lunar dust under natural conditions on the Moon. External factors are considered that result in the formation of the regolith and its most fine-grained component, lunar dust. The properties of the regolith are discussed, and the physical processes occurring during the formation of a near-surface plasma–dust exosphere under natural conditions are considered. Results of the six crewed expeditions of the NASA Apollo program in 1968–1972, with the astronauts performing moonwalks, showed that physical processes caused by anthropogenic activity in the near-surface regions of the Moon lead to much more active dynamics of lunar dust and disturbances in the parameters of the near-surface exosphere than the dynamics of dust particles in their natural state. We discuss examples of the influence of disturbances in the plasma–dust exosphere caused by anthropogenic activity on the service systems of landing vehicles and on the activities and health of astronauts. Unsolved problems that are key to understanding the physical phenomena of the formation and dynamics of the lunar plasma–dust exosphere are discussed. In the last section, we discuss further research avenues and upcoming *in situ* experiments (including domestic ones) to study the plasma–dust exosphere and the dynamics of lunar dust microparticles over the surface of the Moon.

2. Formation and properties of lunar regolith

The surface of the Moon, like the surface of any atmosphereless body in the Solar System, is exposed to external factors: constant bombardment by micrometeoroids and flows of interplanetary plasma, energetic cosmic rays, and solar electromagnetic radiation. These processes are known collectively as *space weathering* [19]. Space weathering leads to the sputtering of surface material and the formation and chemical evolution of regolith — the loose fine-grained upper layer of the Moon. Similar surface erosion processes must be operating on most atmosphereless bodies in the Solar System.

2.1 External factors impacting the Moon

All external factors can be divided into two main categories as regards their physical impact on the surface of the Moon: (1) mechanical, which are random impacts of micrometeoroids on the surface, and (2) electromagnetic, which are the action of the electromagnetic radiation of the Sun, plasma particles of the solar wind, the magnetospheric plasma when the Moon crosses the distant part of the geomagnetic tail, and energetic particles of solar or galactic origin. External factors determine the properties of the regolith and the near-surface exosphere and largely lead to changes in surface topography [20, 21].

2.1.1 Micrometeoroids. Over billions of years, impacts from micrometeoroids have fine-grained the silicate matrix of the Moon's surface into particles with a wide size distribution. The speed of micrometeoroids at distances of the order of one astronomical unit from the Sun can be in the range of 10 to 70 km s^{-1} [22]. Their interaction with the regolith is therefore explosive in nature, and, depending on the relevant processes, several characteristic zones form around the equivalent center of the meteoroid burst [23, 24]. A diagram of the formation of matter evaporation zones below the lunar surface in a high-speed impact is shown in Fig. 1.

Most of the ejecta particles have an initial velocity lower than the Moon's escape velocity (2.4 km s^{-1}) and return to the surface along ballistic trajectories. Micron- and submicron-size secondary particles that are ejected at a near-escape velocity form a highly variable but persistent dust cloud around the Moon. Such rarefied clouds were observed by the LADEE spacecraft near the Moon [25] and by the Galileo spacecraft around four of Jupiter's satellites [26].

Given the high impact velocity and explosive nature of their formation, the particles acquire a highly irregular shape and sharp edges: they are either conglomerates sintered at high temperatures or sphere-like droplets. During the geological epochs, repeated impacts by micrometeorites of various sizes mix and recycle the preformed regolith particles and transport them to various depths. The flow of micrometeorites of cometary and asteroid origin falling on the Moon is estimated at about 10^6 kg per year [27, 28]. The main contribution to the mass flow comes from particles with sizes ranging from 10 nm to 1 mm [22]. When high-speed micrometeoroids hit the lunar surface, an explosion occurs and a crater is formed on the surface. The mass of regolith ejected from the crater can be 1000 times the mass of the impactor itself [29, 30]. A significant portion of the ejected material returns to the lunar surface, forming a layer of regolith. Secondary particles of micron and submicron size that are ejected in a micrometeorite impact with a speed exceeding the orbital velocity for the Moon ($v_1 = 1.68$ km s^{-1}) form a dust cloud around the Moon [28, 31]. At ejection speeds exceeding $v_2 = 2.4$ km s^{-1}, secondary particles permanently leave the Moon. The deposition of dust particles on the lunar surface during bombardment by micrometeorites and by the resulting secondary particles at a speed less than v_1 is estimated as ~ 800 particles/m^2 per year for particles greater than 1 μm in size [29].

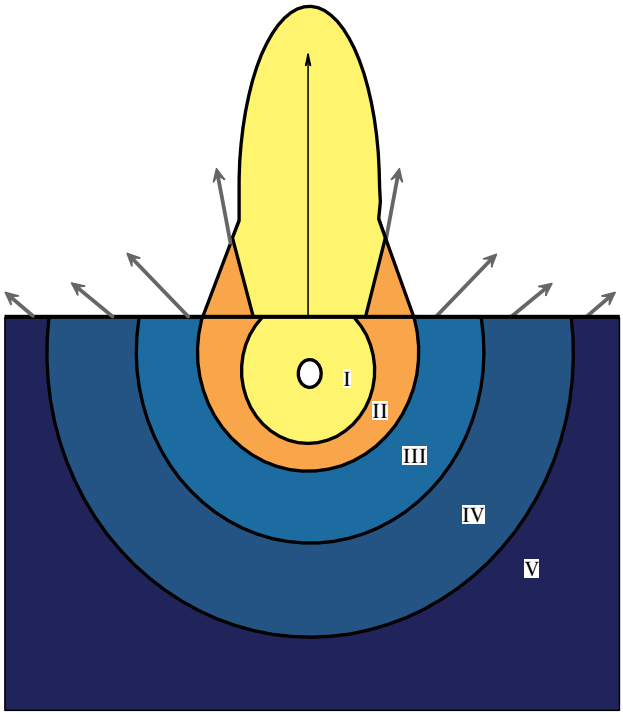

Figure 1. Schematic of formation under the lunar surface of a matter evaporation zone (I), a melting matter zone (II), a zone of destruction of particles that make up the lunar regolith and their irreversible deformations (III), a zone of nonlinear elastic deformations of regolith matter (IV), and zones of linear elastic deformations of regolith matter (V). Circle in zone (I) represents an unperturbed meteoroid at the equivalent center of a meteoroid explosion. Lines from each zone I to V show ejection of matter (including dust particles) at high speeds from surface of the Moon. Same colors as for the corresponding zones shows upward emissions of evaporated and melted matter.

The science program of the Chinese lunar lander Chang'e-3 in 2013–2014 included the deposition of dust particles on a solar battery element with an area of 0.33 cm^2, assessed by measuring the parameters of the electrical signal from that sensor [32, 33]. The solar battery element was located ~ 2 m above the regolith surface. Measurements have shown that the mass of dust settling per unit measuring surface of the sensor per year is 21.4 μg cm^{-2}, which corresponds to an annual average microparticle flux density of $\sim 0.68 \times 10^{-12}$ g cm^{-2} s^{-1}. A comparison of the results with an analysis of the mechanisms for dust-particle lift from the surface of the regolith [34] showed that the leading contribution by mass to the observed fluxes of dust particles could be made by micrometer-size particles originating from the ejections of regolith matter from the lunar surface under micrometeoroid impacts. At the same time, the theoretical estimate turned out to be several times greater than the mass transfer of dust particles measured by the Chang'e-3 mission. Such a difference between experimental data and existing models requires additional analysis.

2.1.2 Interplanetary plasma. Another important factor of external influence on the surface of the Moon is the interplanetary plasma (solar wind) — a flow of electrons and protons from the solar corona, with $\sim 4\%$ of helium nuclei, elements of the group of inert gases and their various isotopes, C and N nuclei, and a small number of other nuclei. Matter of solar origin implanted into the regolith makes a certain contribution to the abundance of rare elements [35] in addition to the main external sources of rare elements on the Moon: meteoroids, asteroids, and comets. The energy of solar wind ions is relatively low (~ 1 keV), and they therefore penetrate only into the uppermost layer of the regolith, no more than a micron thick, causing sputtering in some cases. Radiation damage to the regolith matter is also possible, in the form of the transformation of the crystalline structure into an amorphous one [36]. The average particle speed in a quiet solar wind is approximately 400 km s^{-1}, but it can vary significantly depending on solar activity. The average ion flux in the solar wind is 4.5×10^{12} m^{-2} s^{-1} and is extremely variable with time [37]. Because protons constitute about 95% of ions, this flux is 8.5×10^{-15} kg m^{-2} s^{-1}. Thus, the total amount of solar matter implanted into the lunar regolith is 4.3×10^{25} particles per second, or 0.081 kg s^{-1} (interestingly, this is approximately four times the flow of micrometeorites to the Moon).

In the course of its orbital motion around Earth, the Moon crosses Earth's extended magnetospheric tail; hence, for approximately a third of the lunar day (i.e., ~ 9 Earth days), the Moon experiences the influence of the magnetospheric plasma. A diagram of the orbital motion of the Moon showing its intersection with the bow shock and the geomagnetic tail is presented in Fig. 2. Earth's magnetosphere has a quite complex structure, is extremely dynamical, and largely depends on the parameters of the solar wind and solar activity. The outer zones of Earth's magnetosphere are largely determined by the parameters of the solar wind, whose concentration at 1 AU is about 10 cm^{-3}. When crossing the magnetopause (the boundary of Earth's magnetosphere), the Moon enters the magnetospheric tail plasma and can then be either inside one of the tail lobes or in the low-latitude boundary layer, or in the plasma sheet [38, 39]. In the northern and southern tail lobes, the plasma concentration is very low, 10^{-3} to 10^{-2} cm^{-3} [40]. In the plasma sheet of the magnetospheric tail separating the northern and southern lobes, the plasma concentration is 0.05–0.2 cm^{-3}, but has a high ion temperature (1–5 keV) and a highly variable velocity (10–1000 km s^{-1}) [41]. Plasma instruments from the Apollo 12 and 15 missions provided important information about the influence of magnetospheric plasma on the lunar surface [42, 43]. Model studies of the influence of magnetospheric plasma on the electric charge of the lunar surface and the dynamics of dust particles above the surface were carried out in [44].

With an increase in solar activity, conditions for the acceleration of charged particles can be realized in the solar atmosphere, giving rise to solar cosmic rays (SCRs). The energies of SCR electrons are usually more than 2 keV, and the energies of nuclei are tens of keV/nucleon. The maximum energy of SCR protons depends on the solar activity level and can exceed 10^{10} eV. In addition to protons and electrons, SCRs include heavier nuclei, whose abundance in the high-energy region coincides with their abundance in the solar corona. SCR protons and alpha particles can penetrate into the lunar regolith to a depth of several centimeters. Heavy

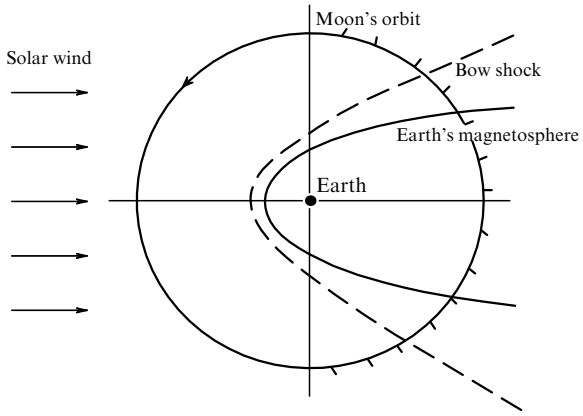

Figure 2. Schematic representation of the Moon's orbit, bow shock, and boundary of Earth's magnetosphere in a plane close to the ecliptic. Ticks on parts of the Moon's orbit indicate intervals that the Moon travels in a time equal to an Earth day.

SCR nuclei are decelerated within a millimeter-thick layer, where they can destroy the atomic structure and leave traces of radiation damage visible with an electron microscope [36].

Galactic cosmic rays (GCRs) have energies greater than 100 MeV, usually of the order of several GeV, but can also reach very high energies of the order of 10^{10} GeV. When interacting with the regolith, heavy GCR nuclei, especially those with a high charge, are decelerated quite rapidly due to ionization losses, within a depth of ~ 0.1 m into the regolith. Radiation impacts on the regolith caused by such nuclei occur at depths of a few centimeters. Lighter GCR nuclei, mainly protons and alpha particles, penetrate much deeper into the regolith, initiating cascades of particles in layers up to several meters in depth. The number of secondary particles in such cascades greatly exceeds the number of primary particles. The dominant particles in a cascade are neutrons with energies below ~ 100 MeV, mainly due to their lack of ionization losses [45].

The processes of radiation modification of the regolith, occurring at different time intervals, lead to changes that can serve as unique chronological markers in studying lunar soil samples; taken together, they yield unique and very extensive information of great importance for solving a wide range of fundamental problems, such as the early history of the Solar System, the nature of the solar wind and the composition of the Sun, the large-scale dynamics of radiation flows in the Solar System, and the radiation history of lunar rocks.

2.1.3 Electromagnetic radiation from the Sun. The impact of the Sun's electromagnetic radiation on the surface of the Moon, and especially its UV spectral component [46], plays an important role in the photoemission of the upper regolith layer. Photoemission leads to accumulation of a positive charge on the illuminated part of the lunar surface and the formation of a double layer of a near-surface electrostatic field.

Solar activity cycles have the greatest influence on the deviation in the solar radiation flux from the average value [47]. Moreover, the flux variability increases at shorter wavelengths, reaching several percent at 200–250 nm and several tens of percent, or even more, for waves shorter than 200 nm. The effects caused by photoemission from the illuminated surface of the lunar regolith are discussed in Section 3.2.

2.2 Properties of the regolith

Most of the information about lunar regolith comes from studies of samples returned to Earth in the 1960s and early 1970s by the Apollo crewed spaceflight missions and robotic spacecraft Luna-16, Luna-20, and Luna-24. Almost half a century later, in 2020, the Chinese mission Chang'e-5 also returned samples of lunar regolith to Earth for laboratory study [48]. All the lunar regolith samples were returned from near-equatorial and middle latitudes of the visible side of the Moon and from elevations. The samples were analyzed within extensive programs of lithological, mineralogical, elemental, granulometric, physical, and other studies (see, e.g., [31, 49–51]).

The upper regolith layer (several millimeters in thickness) is a porous ($> 80\%$) structure [52]. The regolith density increases with depth, and infrared (IR) measurements show that the characteristics of the upper ~ 0.1 m of the regolith are approximately the same over the entire lunar surface, except in recently formed impact craters [53]. The regolith bulk density ranges from 1.04 to 1.90 g cm^{-3} in various samples [4, 54, 55].

2.2.1 Chemical composition. Laboratory analysis of samples returned to Earth shows that lunar rock typically consists of pyroxene, plagioclase, ilmenite, olivine, and small amounts of many other minerals [56]. Such a composition can form as a result of impact processes during micrometeor bombardment. The chemical composition of lunar dust varies across the lunar surface, but on average is about 50% SiO_2, 15% Al_2O_3, 10% CaO, 10% MgO, 5% TiO_2, and 5–15% iron [57].

A key feature of lunar regolith is the presence of greater than expected amounts of elemental, fully reduced metallic iron [58]. The origin of this so-called nanophase metallic iron (np-Fe^0) is associated with high-speed impacts of micrometeorites. As a result of energy release, the material of the lunar surface undergoes not only mechanical destruction but also shock melting and evaporation, which leads to the reduction of iron oxide (Fe_2O_3) to metallic iron [57, 59, 60]. With transmission electron microscopy [61, 62] or ferromagnetic resonance [63], metallic iron in lunar soil and dust particles can be seen as deposits ~ 10 nm in size near the edge of the particles. Deposits of nanophase iron are typically found in aggregates with a high content of SiO_2, sintered under high-speed impacts of micrometeoroids [61, 62]. In this form, nanophase iron cannot affect the chemical activity of lunar dust until these glassy regions are destroyed. It is this feature that allows easily distinguishing between lunar rocks and their terrestrial analogues. Recent studies by the Chang'e-5 lunar lander have provided new data on the abundance of nanophase iron in the lunar regolith [64, 65].

2.2.2 Particle size distribution. Because regolith is the result of impact metamorphism, most of it is made of small and unconsolidated fragments of underlying crystalline rocks covering the entire lunar surface. More than a quarter (by mass) of lunar regolith particles are breccias and glass-bounded aggregates formed from silicates during high-speed impacts of micrometeoroids [66]. Breccia is a coarse-grained rock resulting from impact fragmentation, consisting of fragments of rock sintered at high temperatures. The thickness of the layer of processed regolith is usually 4–5 m in the lunar mare areas and 10–15 m in mountainous areas [66, 67].

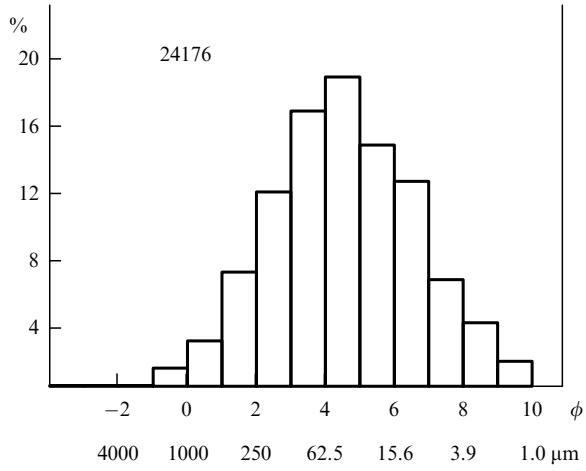

Figure 3. Histogram of size distribution of lunar soil sample no. 24176 returned to Earth by the Luna-24 spacecraft. Vertical axis shows percentage of the mass of particles under study and horizontal axis shows granule size expressed in microns and $\phi = -\log_2(d\,[\text{mm}])$ [69].

Lunar regolith samples returned by the Apollo missions were obtained mainly from the surface (80–90%), as well as from depths ranging from 0.3 to 0.6 m, the particle size distributions being largely identical [68]. Particles less than 1 mm in size make up more than 95% of the regolith mass. The smallest constituent of the regolith, less than 100 μm, is defined as lunar dust. The average particle size ranges from 40 to 100 μm. Such particles make up about half the mass of lunar regolith, most of them having a size from 45 to 80 μm [66, 68]. For nonspherical particles, their size is usually understood as the diameter of an equivalent sphere or circle [31].

The granulometric composition of particles was studied by various methods, including a calibrated sieve, laser analysis, the aerosol diagnostic method, analysis of scanning electron microscope images, and others. Figure 3 illustrates the size distribution of dust particles for sample no. 24176, returned by the Luna-24 automatic station [69]. As noted in [69], the particle sizes of the isolated fractions were monitored using optical and scanning electron microscopes. The results of the analysis showed that approximately 50% of the studied samples consisted of finely dispersed material, i.e., particles less than 70 μm in size; the superfine fraction less than 10 μm in size was about 10% of the mass of the entire analyzed sample, and the thinnest part of the regolith, less than 2 μm in size, made up 1 to 2% by mass [69]. Data on the size distribution of microparticles are important for studying the conditions of detachment of particles from the surface and their subsequent dynamics, for designing effective filtration systems for the human environment, and for studying the toxicological effects of dust on human respiratory functions [70].

Despite the variability in the shape of the particles composing the regolith, their size distribution on the lunar surface satisfies a log-normal law, which is typical of multiple fragmentation [71]. Figure 4 shows experimental data on the particle size distribution from 20 to 500 μm for one of the lunar soil samples returned to Earth by the Apollo missions [5], together with the theoretical Kolmogorov distribution.

The distributions shown in Figs 3 and 4, as well as the results of granulometric measurements of regolith samples

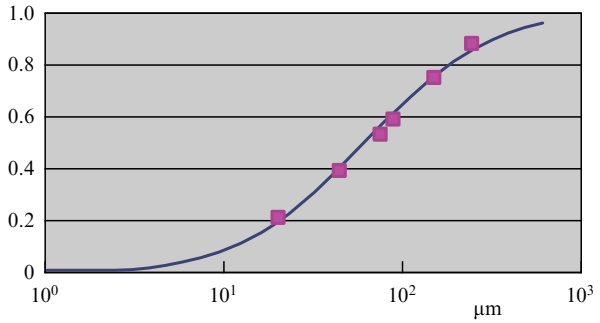

Figure 4. Kolmogorov's theoretical distribution describing observational data of dust particles on surface of the Moon (solid curve). Squares correspond to data in [5].

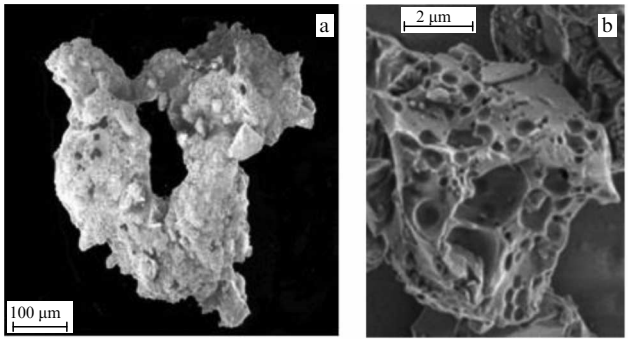

Figure 5. Photographs of two particles of the fine fraction of lunar regolith. (a) Porous glass interspersed with regolith and iron particles. (b) Particle with pores formed as a result of release of volatile components during formation by melting [74].

returned by the Apollo missions [49], show that regolith microparticles with a characteristic size in the range of several tens of micrometers make the main contribution by mass.

It was shown in [72] that, in the case of multiple fragmentation, the Kolmogorov distribution remains valid, at least for particle sizes smaller than or of the order of 100 nm, which allows the distribution of dust particles on the lunar surface deduced from the data in [5] to be extended into that range of sizes. The fact that the distribution of dust particles can be extended to smaller sizes, down to submicrometers and even nanometers, is very significant for theoretical description of dust plasma over the lunar surface [73].

2.2.3 Shape of particles of the fine fraction of lunar soil. The shape of dust particles is generally extremely irregular, with pronounced pointed edges, which markedly distinguishes them from their terrestrial counterparts. The density of individual particles is usually taken to be 2.7–3.0 g cm^{-3} [4]. A rich collection of images of lunar regolith particles is presented in [74]. Figure 5, taken from that collection of images, illustrates a typical agglutinate sample: porous glass with fused rock and iron particles. All dust particles can be morphologically classified into four types: (1) irregular-shaped blocks with sharp corners, (2) glass fragments (flakes), (3) irregular (porous, 'Swiss cheese'-like) pieces, and (4) spherical pieces; it was emphasized that particles of irregular shape typically have pointed corners [70]. The particle shape is mainly oblong, conducive to preferential adhesion of individual particles along their longitudinal axes. As a consequence, the fine fraction of regolith has anisotropic physical properties [75].

2.2.4 Electrical properties of regolith. The electrical properties of dust particles and most silicates of the lunar regolith at zero illumination have an extremely low electrical conductivity, of the order of 10^{-14} S m^{-1} (for regolith) and 10^{-9} S m^{-1} (for consolidated lunar rock) [4, 76]. The regolith electrical conductivity strongly depends on temperature. The average surface temperature is 380 K on the illuminated surface and 120 K during the night; in polar regions, the range of possible surface temperatures can expand significantly [76]. Studies of the effect of irradiation on the electrical conductivity of regolith show that, compared with electrical conductivity in the dark, the surface electrical conductivity increases by approximately 10 times under irradiation in the IR range and by 10^6 times under irradiation in the UV range [77].

The relative dielectric constant is determined by the regolith density ρ and is approximately 1.9^{ρ}, where ρ is expressed in g cm^{-3} [4], and is independent of the mineralogical composition of the regolith. High-frequency electromagnetic losses are determined by the loss tangent (the ratio of the imaginary part of the complex dielectric constant to the real one), depend on the density ρ and the content $(TiO_2 + FeO)$, and are very small for lunar regolith. The extremely low electrical conductivity and small values of the loss tangents indicate that lunar regolith absorbs electromagnetic energy weakly. For example, radio communication on the Moon is possible through a lunar soil layer about 10 m in depth.

As is known, the Moon does not have a dipole magnetic field. However, there are local areas on the Moon with magnetized surface rocks, so-called 'magnetic anomalies' [78]. Solar wind plasma streams, encountering such regions on the lunar surface, can form 'mini-magnetospheres' [79]. In such regions, the interaction of solar wind plasma with the lunar surface is largely controlled by the local magnetic field (these questions are discussed in Section 3.3).

3. Exosphere of the Moon

As is known, the Moon lacks a noticeable atmosphere. However, there is a thin atmosphere in the form of a collisionless gas shell, the so-called exosphere, in which the motion of molecules is controlled mainly by the gravitational field. The values of gas concentration and pressure on the surface of the Moon are apparently comparable to similar values on the surfaces of some other atmosphereless bodies of the Solar System, e.g., Mercury, large asteroids, and a number of satellites of the giant planets. Along with a neutral atmosphere, the Moon also has an ionosphere. Similarly to the neutral lunar atmosphere, the chemical composition of the ionosphere is determined by its interaction with the lunar surface.

3.1 Ionosphere and atmosphere

3.1.1 Ionosphere of the Moon. The first convincing evidence of the existence of an ionosphere around the Moon was obtained in the 1970s by radio occultation methods using the Soviet probes Luna-19 and Luna-24 [80]. These measurements showed that the ion concentration can be ~ 100 cm^{-3} [81], with a peak electron concentration of 500 to 1000 cm^{-3} and with a characteristic altitude of $\sim$ 10–30 km [82]. Recent studies of the lunar ionosphere using the Japanese Kaguya lunar satellite [83] have shown an average concentration peak

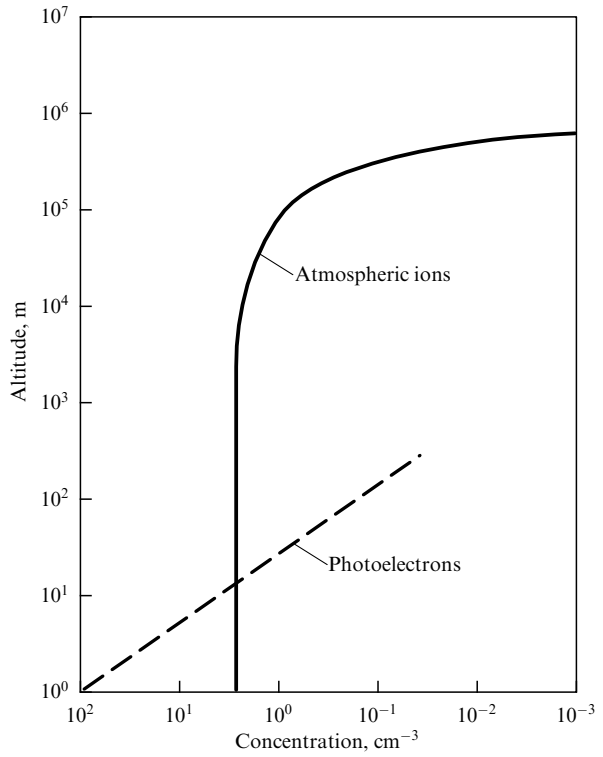

Figure 6. Dependences of concentrations of photoelectrons and atmospheric ions in ionosphere of the Moon according to data from SIDE experiments [87].

of ~ 300 cm^{-3} at an altitude of 15 km with a gradual decrease both at higher altitudes and towards the surface. Such high concentrations are not consistent with the assumed physical mechanism of ionosphere formation, according to which the ion concentration is ~ 1 cm^{-3}, despite the fairly high concentration of exospheric neutrals on the day side of the Moon (10^5 cm^{-3}), the long process of photoionization (10 to 100 days), and the short time (~ 1 s) of ion loss due to capture by the solar wind [84]. This contradiction was discussed in [85], where it was shown that photoelectrons emitted by charged dust particles located at high altitudes may be responsible for the results of radio occultation measurements.

The lunar ionosphere contains ions from various sources: generated by the lunar atmosphere, coming from the solar wind, coming from Earth's magnetosphere, and correlated in time with signals from seismic detectors, which later allowed such particles to be identified as ions associated with meteoroid impacts [84]. Almost all of these data were obtained during the lunar day. The mass/charge ratios $m/q = 20$–28 and $m/q = 40$–44 for ions detected by the SIDE instruments were respectively assigned to ionized ^{20}Ne and ^{40}Ar atoms that are part of the natural lunar atmosphere. Assuming an argon composition of the atmosphere, SIDE data allows describing the lunar atmosphere using an exponential (barometric) formula with a characteristic height of about 40 km.

During the day, along with ions, a shell of photoelectrons several hundred meters in thickness is present near the surface of the Moon [86]. Located above this layer is a region of ions originating from the neutral lunar atmosphere. After formation, such ions move either toward the surface of the Moon or away from it, accelerating along the lines of the interplanetary electric field. Figure 6 shows the concentrations of photoelectrons and atmospheric ions in the lunar ionosphere according to the SIDE data [87].

Table 1. Concentration of main components of lunar atmosphere on the day and night sides of the Moon [87].

Atmosphere component	Daytime, cm^{-3}	Night time, cm^{-3}
H_2	4×10^3	1.2×10^4
^{4}He	2×10^3	4×10^4
^{20}Ne	4×10^3	1×10^5
^{36}Ar	1×10^2	3×10^3
^{40}Ar	1.6×10^3	4×10^4
CO	3×10^5	$< 10^3$
CO_2	6×10^5	$< 10^3$
CH_4	7×10^4	$< 10^3$
Na	6.7×10	
K	1.5×10	

3.1.2 Neutral atmosphere of the Moon. The lunar atmosphere is extremely rarefied. The gas concentration is only about 2×10^5 molecules cm^{-3} during the lunar night, and even less during the lunar day: approximately 10^4 molecules cm^{-3} [88]. Given that this is 14 orders of magnitude smaller than Earth's atmosphere, the Moon is often considered to have no atmosphere at all.

Experiments to study the composition and bulk properties of the neutral lunar atmosphere were carried out during the NASA Apollo program [76, 89]. However, basic ideas about the lunar atmosphere are based on theory. This is because the total mass of the lunar atmosphere is very small, only 10^4 kg. Approximately the same mass of gas was ejected by each Apollo lander as it descended to and ascended from the lunar surface. Thus, the six Apollo missions returned six times more gas to the Moon than the mass of the atmosphere itself [90].

A breakthrough in the study of the lunar atmosphere was the discovery of the D_2 line emission from atomic K and then Na, made by observations from Earth in the late 1980s [91, 92]. The total concentration of Na and K in the lunar atmosphere is only $\sim 10^2$ cm^{-3}. It may seem that these elements make only a minor contribution to the lunar atmosphere, but the possibility of detecting Na and K from Earth makes them very valuable sources of information about it. The most common component of the lunar atmosphere is CO_2 on the day side and Ne on the night side. In Table 1, we present the concentrations of the main components of the lunar atmosphere on the day and night sides of the Moon, obtained from measurements carried out during the Apollo missions. In Table 2, we give the total mass of the main components [87].

Table 2. Estimation of total mass of most common components of lunar atmosphere [87].

Atmosphere component	Weight, kg
CO_2	5200
CO	2000
CH_4	640
Ne, Ar	< 500

3.1.3 Sources of and losses from lunar atmosphere. The sources and the loss mechanisms of various atmospheric components are important characteristics for understanding the formation and existence of an atmosphere. An estimate of the characteristic rate of loss of the lunar atmosphere is $\sim 10^{-2}$ kg s^{-1} [90]. This value (compared to the total mass of the atmosphere of $\sim 10^4$ kg) means that losses actually control the dynamics of the lunar atmosphere and determine its equilibrium concentration.

At least four mechanisms of loss have been identified for the lunar atmosphere. (1) The primary one is so-called *gravitational escape*. Because the lunar atmosphere is an exosphere where the mean free path of atoms and molecules is much greater than the characteristic height of the atmosphere, atoms or molecules moving away from the Moon at speeds exceeding the escape velocity (2.38 km s^{-1} for the Moon) typically go into outer space. (2) The next loss mechanism is *ionization losses*, which occur because ionized atoms and molecules in the lunar atmosphere are entrained by the electric field of the solar wind and accelerated in it to speeds of the order of the escape velocity. Ionization of neutral atoms and molecules occurs under the influence of solar UV radiation and charge exchange. All these processes occur with varying degrees of intensity in accordance with the 11-year solar cycle and, to a lesser degree, with the 28-day rotation of the Sun. In addition, there are (3) *chemical losses* and (4) *condensation*. The most important type of chemical loss involves collisions of atmospheric atoms and molecules with the lunar surface, which can lead to chemical reactions that bind an atom or a molecule to the surface. Less important are losses due to chemical reactions that occur when gas molecules collide. Although the lunar atmosphere is an exosphere, atomic collisions can still occur. However, the cross sections of chemical reactions occurring in pairwise collisions of the many components of the lunar atmosphere (for example, Ar – X, He – X, Na – Na, Na – K, and K – K) are quite low, which further reduces the (already low) efficiency of this atmosphere loss process.

A significant loss mechanism in the lunar atmosphere is due to condensation. The condensation process manifests itself, e.g., as a result of collisions of high-speed meteoroids with the lunar surface. The rate of such collisions (number per unit time) is very significant (see, e.g., [93]). In a zone around the impact epicenter, matter evaporates and rises at speeds exceeding the escape velocity for the Moon. A cloud of evaporated matter expanding into empty space is subject to the process of condensation [94], and a significant part (tens of percent) of this matter is indeed condensed. Particles of condensed matter rise above the lunar surface at speeds exceeding the escape velocity for the Moon, and thus leave it, going into outer space. However, such losses should instead be classified as the loss of regolith matter rather than the atmosphere.

The sources that replenish the lunar atmosphere fall into five main categories: thermal sources, sputtering due to the external influence of meteoroids, chemical and meteorite sources, and internal emissions. These issues are discussed in detail in [84]. We note that, first, different types of sources are important for different components of the atmosphere, and, second, there is no single source that supports the entire atmosphere with all its components.

Thermal sources, sometimes called thermal desorption, involve the sublimation of matter in the uppermost (near-surface) layer of the lunar regolith, which is influenced by the daily cycle of surface temperature oscillations. These sources are concentrated mainly along the lunar terminator in the morning and, to a lesser extent, on the daytime side of the Moon.

Sputtering sources are associated with ejections of particles from crystal lattice sites in several upper monolayers of the lunar surface under discrete pulsed actions (for example, impacts of solar wind particles). All types of sputtering on surfaces are complex and difficult to analyze precisely, which prevents quantification of the material yield due to sputtering on the Moon.

Chemical sources include chemical sputtering, which occurs when a chemical reaction on the lunar surface (for example, due to incident protons from the solar wind) has enough extra energy for desorption. This process seems to provide a high yield of atomized volatiles.

Meteorite sources are associated with impacts of meteoroids incident on the surface of the Moon at speeds of the order of tens of kilometers per second. Among the neutral atoms of the atmosphere from this source, volatile substances such as alkalis, sulfur, H_2O, and other components, mainly in the form of molecular fragments, are expected to be dominant.

Internal emissions may be associated with volcanism (which, however, is presently nonexistent on the Moon), diffusion in the lunar crust, or leaks caused by seismic impacts.

3.2 Processes on regolith surface under the influence of external factors

On the surface of the Moon, as on any large body surrounded by plasma, an equilibrium electric potential is established that prevents an increase in charge due to the constantly oncoming plasma flow. This process leads to the formation of a near-surface region of nonneutral plasma, bounded by two oppositely charged layers. On the side of the Moon illuminated by the Sun, such a near-surface region of nonneutral plasma, the so-called 'double sheet,' forms due to the interaction of the incoming flow of solar wind plasma with the regolith surface. The transverse size of the double sheet is of the order of the Debye radius [95]. The parameters of the double sheet plasma are determined by external factors, e.g., plasma concentration, thermal velocities of plasma particles, and electrical conductivity of the regolith; on the sunlit side of the Moon, for example, the thickness of such a layer is about 1 m [5]. The near-surface plasma forms under the action of solar radiation on the lunar regolith as a result of the photoelectric effect, the incoming plasma flows of the solar wind (or the tail of Earth's magnetosphere when it is crossed by the Moon), and the effects of proton backscattering [96], secondary electron emission, and sputtering. For the Moon and most other atmosphereless bodies, the rate of photoemission under solar illumination is much greater than the rate of absorption of solar wind electrons by the regolith, and the regolith surface then acquires a positive charge.

Electron photoemission is generally the main process responsible for charging the surface layer of the regolith on the illuminated side of the Moon. Incident photons with energies exceeding the work function of the lunar surface material cause photoemission of electrons. The work function of lunar regolith matter and its quantum yield, which characterizes the number of electrons knocked out from the surface by one photon, were experimentally studied in laboratory conditions [97, 98]. However, the authors noted that these studies were carried out in an inert atmosphere

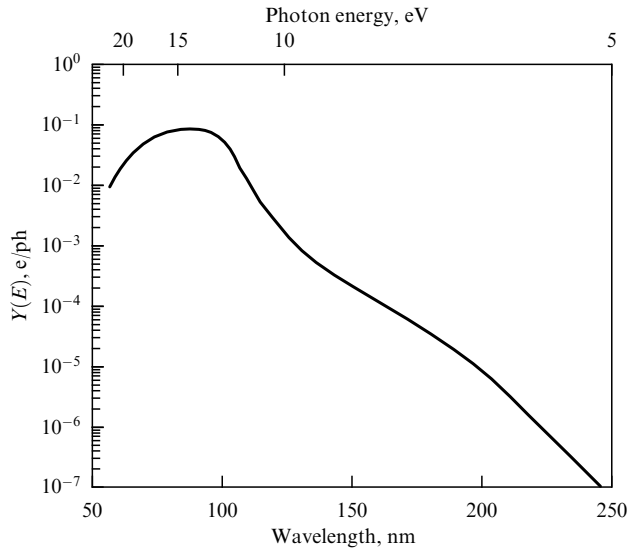

Figure 7. Quantum yield for two lunar regolith samples (nos. 14259.116 and 15021.98) [98].

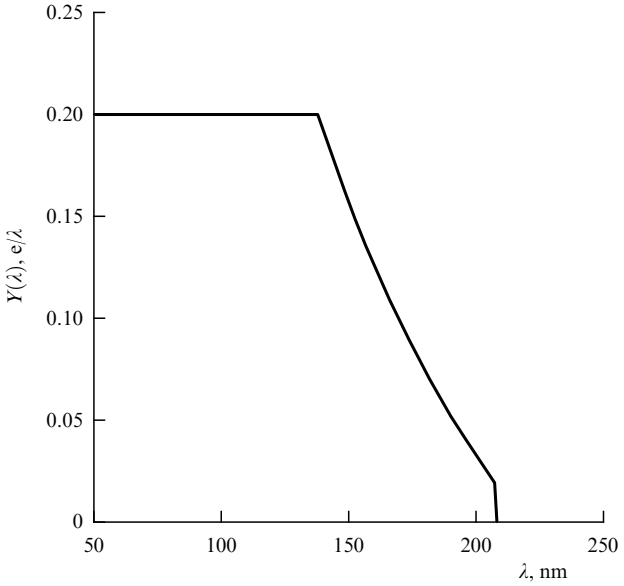

Figure 8. Results of a model analysis of quantum yield of lunar regolith [99].

containing impurities, and its electrical properties could significantly affect the results. In [97], only one sample was studied, which, according to the authors, cannot be sufficiently representative to arrive at definitive conclusions, and in [98], rather small particles were studied, which could affect the obtained quantum yield values. Figure 7 shows the differential photoelectron flux obtained as a result of an experimental study of two samples of lunar regolith returned to Earth by the Apollo missions [98]. Figure 8 shows the results of a model analysis of such a dependence, carried out in [99].

It is clear from the presented dependences that they differ significantly. Insufficiently accurate data on the quantum yield of photoelectrons of the lunar regolith and significant variations in the photon energy at different levels of solar activity [100] in theoretical analyses lead to significant uncertainties in the estimates of surface potentials on the illuminated side of the Moon. It is therefore important to determine these and other electrophysical characteristics of the lunar regolith directly on the Moon or in laboratory conditions in an environment as close to the lunar one as possible.

Currently, the work function of lunar regolith is generally accepted to be in the range of 5–6 eV [101]. These work function values are used, together with the dependence of the quantum yield value on the photon energy given in [98] and [99], in studies where the effects of photoemission near the lunar surface have to be taken into account.

For example, the results of calculating the photoelectron layer above the illuminated surface of the regolith in [97] are 0.78 m for its thickness and ~ 130 cm^{-3} for its concentration. But when using the data in [99], the concentration of photoelectrons reaches 2×10^5 cm^{-3}, and the photoelectron layer thickness (determined by the condition that the concentration of solar wind electrons in it is much less than the concentration of photoelectrons) reaches several tens of meters [102]. The work function and quantum yield of the lunar regolith determine the photoelectron energy distribution function $\Phi_e(E_e)$, which can be derived in a standard way by calculating the flux density of photoelectrons emitted by an irradiated solid body,

$$\Phi_e(E_e)\,dE_e = 2\cos\theta\sqrt{\frac{2m_e}{E_e}}\int_{E_e+W}^{\infty} Y(E_{ph})F_{ph}\,d\rho\,dE_{ph}\,, \quad (1)$$

where E_e is the photoelectron energy, E_{ph} is the photon energy, W is photoemission work function, θ is the angle between the local normal and the direction to the Sun, m_e is the electron mass, $Y(E_{ph})$ is the quantum yield depending on the photon energy, and $F_{ph}\,dE_{ph}$ is the number of solar radiation photons with energy E_{ph} in the interval dE_{ph}, crossing a unit area perpendicular to the direction of photon motion per unit time. The coefficient 2 appears on the right-hand side of (1), because the number of electrons leaving the surface of a solid and the number of electrons absorbed by it are equal in a stationary state. In deriving formula (1), the possible anisotropy of the photoelectron distribution function in velocity space, caused by the roughness of the lunar surface, was neglected. The probability that an electron with energy E_e is emitted within the energy interval dE_e due to the absorption of a photon of energy E_{ph} is given by [99]

$$d\rho = \frac{6(E_m - E_e)}{E_m^3}\,E_e\,dE_e\,, \quad 0 \leqslant E_e \leqslant E_m = E_{ph} - W. \quad (2)$$

It was shown in [103] that the photoelectron distribution function differs significantly from the usual Maxwellian distribution. Figure 9 shows the distribution functions $f_e(E_e) = \Phi_e(E_e)/N_0$, where N_0 is the photoelectron concentration on the surface of the Moon calculated for the data corresponding to quantum efficiency [98] and different levels of solar activity. The total distribution function $f_e(E_e)$ is a superposition of the distribution function of photoelectrons ejected by photons with energies close to the work function and having a temperature in the range of 0.1–0.2 eV, and the distribution function of photoelectrons associated with the Ly-α hydrogen line (10.2 eV) in the solar radiation spectrum and having a temperature of the order of 1 eV. Hence, photoelectrons with energies both of the order of 1 eV and of the order of 0.1 eV should be observed.

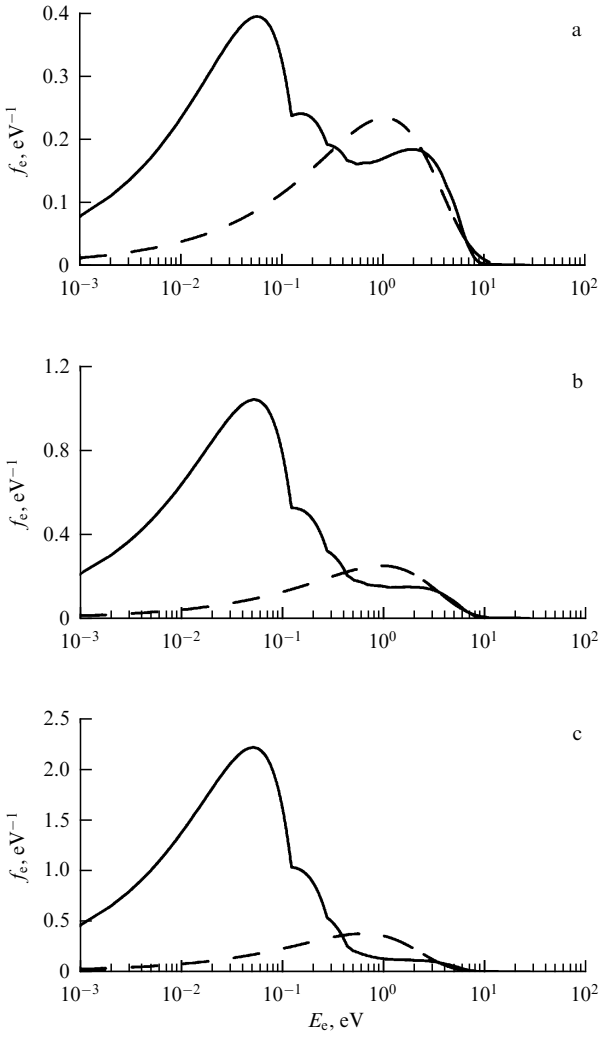

Figure 9. Energy distribution functions of photoelectrons $f_e(E_e)$ (solid curves) near illuminated part of lunar surface, corresponding to (a) a solar flare of class X28, (b) a solar maximum, and (c) a solar minimum. Lunar regolith work function is $W = 6$ eV, and quantum yield is determined by an experimental dependence [98]. Dashed curves show Maxwellian distributions calculated for values of average photoelectron energy characterizing corresponding distributions represented by solid curves [103].

The energy spectra of emitted photoelectrons are determined by the spectrum of incident photons times the photoemission quantum yield as a function of photon energy (see Eqn (1)). Depending on the solar activity level, solar radiation fluxes can change dramatically, especially in the photon energy range above 10 eV [100, 104]. Therefore, the photoelectron spectra on the illuminated surface of the Moon (as well as on other atmosphereless bodies) are extremely variable and, as already noted, very sensitive to the quantum yield value [100, 103]. The model distribution of photoelectrons over the lunar regolith illuminated by the Sun was considered in several studies (see, e.g., [10, 12, 103, 105, 106]). In a recent study [107], it was shown using an analytic approach [108] that the energy distribution of photoelectrons in a stationary state largely depends on the charge and temperature of the lunar surface. Conversely, the energy distribution of photoelectrons is critical for deciding how large the dayside surface potential is in the solar wind and in the magnetotail [107, 109].

3.2.1 Interaction of interplanetary plasma with regolith. Besides photoemission, electron and ion currents created by the incoming flow of solar wind plasma or magnetospheric plasma can also make a certain contribution to the formation of the surface potential when the Moon crosses the distant tail of Earth's magnetosphere. Typically, the solar wind plasma flux onto the lunar surface is 10^8 ion cm^{-2} s^{-1} in the energy range of 350–1200 eV amu^{-1}. Under the action of interplanetary plasma flows on the regolith surface, ion backscattering, surface sputtering, and secondary electron emission of the regolith can also make some (although much less, at the level of several percent) contribution to the formation of the regolith surface potential.

When solar wind plasma interacts with lunar regolith, most of the ions are absorbed by the regolith material. Studies of the interaction of the solar wind with the Moon by the spacecraft Chandrayaan-1 (2008, India), Kaguya (2007, Japan), Chang'e-1 (2007, China), and Artemis (2007, USA) showed in [110] that a significant portion of solar ions ($\sim$ 10–20%) capture electrons and are scattered in space in the form of neutral atoms [96, 111, 112]. A small part of the H^+ ions ($\sim$ 0.1–1.0%) are reflected from the surface, retaining a positive charge [113]. As regards solar wind electrons, their backscattering coefficient depends on their speed and surface material; the resulting albedo for such particles with energies of $\sim$ 100 eV is $\sim$ 10–30% [114].

Sputtering of lunar regolith particles by solar wind protons and heavier ions is a process leading to erosion of the upper layer of the regolith and is therefore one of the sources behind the formation of the atmosphere and exosphere of the Moon [115, 116]. This problem was briefly discussed above in the analysis of the sources of the lunar atmosphere. Here, we only recall that the main processes involving atomic sputtering of regolith, in addition to micrometeoroid impacts, are atomic sputtering of regolith material by the solar wind flow and photon-stimulated desorption [117–119].

When incident particles of interplanetary plasma interact with surface material, surface atoms can be excited, which is accompanied by secondary electron emission. The efficiency of secondary electron emission depends on the energy of the incident particle and the surface material. Higher-energy incident particles can reach deeper layers and release more electrons, which, however, are less likely to leave the material than the secondary electrons produced at a shallower depth. Therefore, the functions characterizing the secondary electron emission coefficient contain peaks corresponding to the primary electron energies of several hundred eV for an electron impact and $\sim$ 10–100 keV for a proton impact. The distributions of secondary electrons are Maxwellian with characteristic energies of several eV [120]. In some cases, the secondary electron emission coefficient can be greater than unity [121].

However, we note once again that, under illumination conditions, the average charge of the lunar surface is determined by photoemission, and the role of plasma flows, and even more so of secondary electron emission, is insignificant [98].

3.2.2 Regolith surface potential. The lunar surface is charged, and a near-surface electric field forms near the Moon as the result of a complex interplay of external factors acting on the surface of the regolith, including, first and foremost, solar UV radiation, flows of electrons and ions of the solar wind (or

magnetospheric plasma when the Moon crosses the geomagnetic tail), and collisions of high-speed micrometeoroids with the surface.

The electric potential of the regolith surface under the influence of solar radiation is established when the sum of the principal currents that affect the potential is equal to zero. These are the photoemission of electrons J_{pe} and the fluxes of plasma electrons J_e, plasma ions J_i, and secondary electrons J_{sec} (which arise as a result of the impact of electrons of the incoming plasma flow on the surface of the regolith, as we discuss below). On the illuminated side of the Moon, the concentration of photoelectrons is usually more than an order of magnitude higher than that of solar wind plasma, and hence the surface potential on the illuminated side is positive [122].

The surface potential was determined during the NASA Apollo program [123, 124]. In accordance with measurement data, the potential of the illuminated part of the regolith surface is of the order of +10 V at solar zenith angles up to $\theta \sim 20^\circ - 45^\circ$ (where θ is the angle between the local normal and the direction to the Sun). Because the lunar regolith surface is almost insulating, the acquired surface potential can persist for a long time [125, 126]. A double (plasma) sheet with an electric field E then appears between the charged surface of the regolith and the surrounding quasineutral plasma. The characteristic thickness of such a sheet is of the order of the Debye length, which is about 1 m for the Moon [5]. With an increase in the solar zenith angle to $\theta > 45^\circ$, the surface potential rapidly decreases: at the terminator, it becomes negative and can reach −100 V [123].

On the night side of the Moon, as for any atmosphereless nonconducting celestial body, the incident solar wind flow creates an area with an extremely low concentration and low velocity of plasma. In this case, an analogue of the double sheet is assumed to be a region with a transverse size of the order of the Moon's diameter [95]. Given that the thermal velocities of electrons V_{Te} are much greater than those of positive ions V_{Ti}, it was analytically shown in [8] that the potential of the regolith surface on the night side of the Moon must be negative.

Measurements of the electrical potential of the lunar regolith surface carried out from the Lunar Prospector lunar orbiter [127] showed that the regolith potential is negative on the night side of the Moon, being equal to about −200 V near the boundary of the shadow and about −100 V in the central part of the lunar night [128]. However, when the Moon crosses the geomagnetic tail in the region of the current sheet, as well as in the solar wind during energetic solar flares, the negative potential of the regolith on the night side of the Moon can reach several kilovolts [129]. The structure of the double sheet on the night side of the Moon depends on the direction of the solar wind plasma flows relative to the vector of the interplanetary magnetic field and the electrical conductivity of the regolith, which, although extremely low, determines the surface currents and hence the average surface potential [8].

From the standpoint of electrostatic processes, a special zone on the surface of an atmosphereless body is the terminator zone — the boundary of the illuminated and shaded regolith surfaces. It was in the terminator zone that several American and Soviet lunar landers recorded LHG [1, 2, 130] caused by the reflection of solar radiation from dust particles that presumably levitate in near-surface electric fields (see, e.g., [126]). Many papers have been devoted to studying the features of the terminator zone from the standpoint of the acquisition of an electric charge by the regolith surface and the structure of the double sheet (see, e.g., [9, 32, 131–137]).

Above the illuminated part of the Moon, as already noted, the main components of the near-surface plasma are photoelectrons and positively charged dust particles, while, above the night part, the main contribution is made by solar-wind electrons. Moreover, the concentration of electrons above the illuminated part is always significantly higher than above the night side of the Moon. As a result, the terminator zone contains a region analogous to a plasma sheet, in which significant electric fields can arise (~ 300 V m^{-1}) [138].

Surface inhomogeneities can also play an important role in producing significant electric fields in the terminator region [139–141]. It was shown in [9] that conditions for the formation of strong local electric fields are created near the terminator. Indeed, in the lunar surface areas near the terminator, the value of the solar zenith angle θ is close to 90°, and therefore sharp local alterations between light and shadow exist at the boundary of acute local inhomogeneities of the regolith surface, e.g., near craters or hills of various scales. This leads to the formation of a large local potential gradient, whose magnitude depends on the slope of the local heterogeneity of the regolith surface (i.e., on θ_z). The extremely low conductivity of the lunar regolith supports the formation of a large potential difference on a scale much shorter than the Debye radius [9]. The estimates in that paper show that the resultant local electric fields become strong enough for dust particles about 1 mm in size to be lifted above the surface. The proposed mechanism is effective only on the night side after sunset and close enough to the terminator. Far from the terminator on the night side, the flow of charged particles hitting the surface is so insignificant that the process of raising dust becomes too weak.

To conclude the discussion of the formation of the lunar regolith surface potential, we emphasize that the relevant physical processes depend on the solar activity, lighting conditions, influence of the plasma of Earth's magnetosphere, and characteristics of the regolith surface. Despite the large number of studies devoted to the above problems, additional experimental and theoretical work is needed to clarify the values of the potential and elucidate the basic physical processes leading to its formation. The most critical area, which hosts a large number of unresolved issues, is that of the lunar terminator — the boundary of light and shadow.

3.3 Near-surface plasma–dust environment

It has become generally accepted by now that dust above the lunar surface is an integral part of the plasma–dust system of the lunar exosphere. We qualitatively describe the general picture of physical processes under the influence of external factors on the surface of the regolith and the formation of the plasma–dust exosphere of the Moon: electromagnetic radiation of the Sun, solar-wind plasma, and plasma of the tail of Earth's magnetosphere. Figure 10 shows a simplified diagram of the influence of external factors on the regolith surface in the formation of the plasma–dust environment.

On the illuminated side of the Moon, the regolith surface acquires an electric charge due to the photoelectric effect (the contribution of the solar wind plasma flow is usually much less than the photoelectric effect), giving rise to a near-surface plasma sheet and an electric field E. Those dust particles lying on the regolith surface for which the electrostatic force F_c

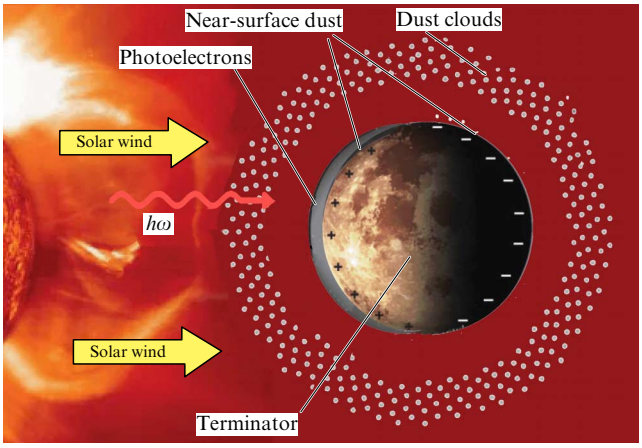

Figure 10. Main elements characterizing plasma–dust system above lunar surface: terminator, photoelectrons, near-surface dust, high-altitude dust, solar radiation photons ($\hbar\omega$), and solar wind.

exceeds the van der Waals adhesion force $F_{\rm vdW}$ and the force of gravity $F_{\rm g}$ lift off the surface and become components of the plasma–dust exosphere (lofting). Dust particles floating above the surface of the Moon also emit photoelectrons when they absorb UV radiation. All dust particles lying on and hovering above the regolith surface constantly acquire charge as a result of the photoelectric effect and the absorption of photoelectrons. Whenever the Moon is in the tail of Earth's magnetosphere or when considering plasma–dust processes on the night side of the Moon, external influences on the regolith change, and the mechanisms for the regolith microparticles to acquire charge also change, but a plasma sheet is still formed above the regolith surface, together with a near-surface electric field and hence a plasma–dust exosphere, whose characteristics are determined by external influences and the electrical properties of the regolith.

3.3.1 Observations of lunar dust dynamics. One of the important and not fully explored factors of external influence on the surface of the Moon is the dynamics of microparticles of the lunar regolith, the so-called lunar dust. The first indications of the presence of dust in the near-surface layer above the Moon were obtained by the Surveyor robotic landing spacecraft, which used a TV camera to obtain images of the lunar horizon after sunset [2] (Fig. 11). These images reveal a near-surface glow over the region of the lunar terminator with a maximum brightness of 0.26 cd cm^{-2}, with characteristic heights of $\sim$ 10–30 cm. The authors of [2] concluded that the observed glow may be due to the scattering of sunlight by suspended (levitating) charged dust particles with dimensions $a \sim 5$ μm above the surface in an electric field exceeding several hundred V cm^{-1}.

The existence of lunar dust at higher altitudes was proved using a two-channel (2700 Å and 5400 Å) astrophotometer installed aboard Lunokhod-2, which recorded light scattering [130]. Estimates based on these measurements indicated that the cloud of dust scattering sunlight was located 260 m above the lunar surface. In addition, the Apollo mission astronauts took photographs and made sketches of visual observations during the circumlunar flight phase. Some of these sketches are presented in Fig. 12 [142]. Later, as part of the Clementine mission, images were also obtained indicating the existence of a glow in the lunar horizon region, which, as the authors of

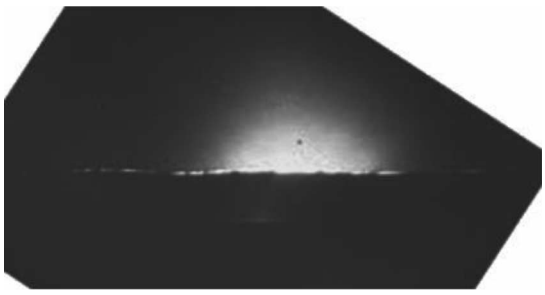

Figure 11. Raw image of LHG obtained by the American Surveyor-6 lander (part of a photo from the National Space Science Data Center) [5].

[143] believe, is associated with the rise of dust due to electrostatic processes.

The presence of dust in the lunar exosphere is also indirectly evidenced by data from the Soviet missions Luna-19 and Luna-22. High electron concentrations in the lunar ionosphere, obtained by the radio occultation method [82] (see Section 2.1), can be caused by charged dust particles at altitudes of 5 to 10 km above the Moon [85].

The first direct detection of dust particles above the lunar surface dates back to the LEAM (Lunar Ejecta and Meteorite) experiment conducted on the lunar surface by the Apollo 17 astronauts [3]. Using the LEAM installation, they could obtain data on fairly intense particle flows with velocities $v \sim 100$–1000 m s^{-1}, whose charge was typically $Q > 10^{-12}$ C ($> 10^7 e$).

Actual evidence of the lofting of regolith microparticles above the lunar surface, obtained at the early stages of lunar exploration [5], led to the development of theoretical and experimental work aimed at explaining plasma–dust processes in the near-surface exosphere of the Moon. Dynamical

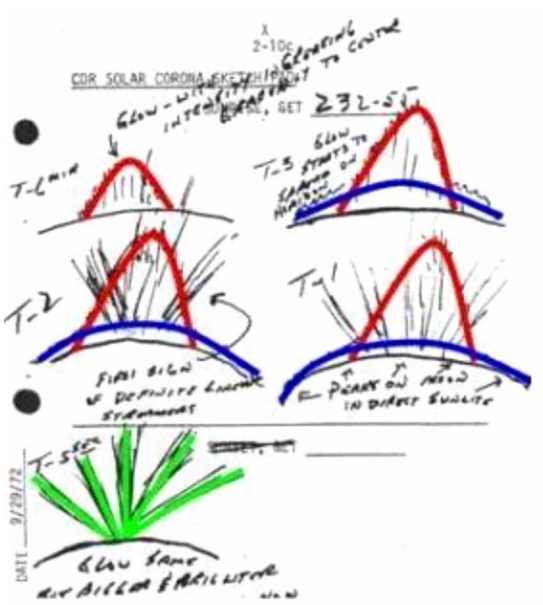

Figure 12. Part of a sketch of the sunrise on the Moon seen from the Apollo 17 spacecraft in lunar orbit. Coronal and zodiacal luminosity is marked in red; blue: lunar dawns, possibly caused by dust in the lunar exosphere; green: possible light streamers (twilight rays) formed by shadowed and diffused light [142].

models of the behavior of dust particles over the surface of the Moon acted upon by electrostatic forces were developed in theoretical and experimental studies [10–14, 105, 144] and elsewhere.

3.3.2 Distribution of dust in near-surface exosphere. A theoretical model of the distribution of dust particles and electrons in the near-surface layer of the illuminated part of the Moon was proposed in [12, 73, 103]. Calculations were carried out in terms of the angle θ between the local normal and the direction to the Sun, and the photoemission work function value $W = W_R \approx 6$ eV was used for different estimates of the quantum yield. To describe the plasma–dust system in the near-surface layer of the illuminated part of the Moon, the charging of dust particles above the lunar surface was calculated with the influence of photoelectrons in the double surface layer, electrons and ions of the solar wind, and the photoelectric effect on dust particles taken into account [73]. The influence of light pressure on the dynamics of dust particles was not considered because, according to the estimates in [73] based on a comparison of the electrostatic force acting on a dust particle near the surface of the Moon and the force of light pressure, this effect is felt only by particles whose size is well below 1 nm.

As noted above, the calculations took photoelectrons both from the lunar surface and from the surfaces of dust particles floating above the Moon into account. Considering photoelectrons from the surfaces of dust particles requires a self-consistent description, because the presence of photoelectrons affects the distributions of dust particles, while the distribution of dust particles determines the number of photoelectrons. Due to the self-consistent nature of the problem, it can be solved only numerically. To find the concentration of photoelectrons over the lunar surface, a system of equations is to be solved that consists of a stationary kinetic equation for the photoelectron distribution function and the Poisson equation for the electrostatic potential with the corresponding boundary conditions characterizing the behavior of the potential near the lunar surface and at an infinite distance from it. To find the distribution function of photoelectrons near the lunar surface, the number of near-surface electrons knocked out by photons via the photoelectric effect is calculated using the solar radiation spectrum [145, 146], with due account for the decrease in the work function and the increase in the quantum yield of regolith photoemission in a hydrogen monolayer on dust particles on the lunar surface [147]. In the zeroth approximation, when the photoelectrons originating from the dust particle surfaces are disregarded, it turns out that the distribution of photoelectrons with respect to velocity near the surface of the Moon can be approximated by a Maxwellian distribution with the photoelectron temperature $T_{e,\,ph}$ and the concentration N_0. The behavior of dust particles in the near-surface layer is described by equations that take their dynamics and charging into account:

$$m_d \frac{d^2h}{dt^2} = q_d E(h,\theta) - m_d g_M\,, \tag{3}$$

$$\frac{dq_d}{dt} = I_e(q_d) + I_i(q_d) - I_{ph}(q_d) + I_{e,\,ph}(q_d)\,, \tag{4}$$

where h is the height above the lunar surface, m_d is the mass of a dust particle, q_d is its charge, g_M is the acceleration of gravity near the lunar surface, $I_e(q_d)$ and $I_i(q_d)$ are microscopic currents of solar wind electrons and ions onto a dust particle, $I_{ph}(q_d)$ is the photocurrent of electrons from a dust particle due to its interaction with solar radiation, and $I_{e,\,ph}(q_d)$ is the current of photoelectrons onto a dust particle (see, e.g., [73]). The minus sign in front of the third term on the right-hand side of (4) means that photoelectrons described by this term leave the surface of the dust particle, while the plasma particles described by the first, second, and fourth terms, conversely, are absorbed on it.

Calculations with system of equations (3), (4), in particular, allow determining the size distribution of dust particles floating above the Moon. The probability of a particle being present at a certain height can then be calculated (it is proportional to the time spent by the particle at a given height). This probability is multiplied by a normalization factor, which is calculated so as to provide a suitable description of the size distribution of lunar dust on the surface (at zero height), given in Section 2.2 (see Fig. 4). As a result, in Fig. 13, we show the distribution of dust particles of different characteristic sizes along the height above the lunar regolith surface. Figures 13a–c show histograms describing the results of calculations of dust particle concentrations above the surface in the polar region of the Moon for the angles θ between the local normal and the direction to the Sun equal to 77°, 82°, and 87°, under the assumption of a smooth surface of the Moon (without hills and depressions) approximately corresponding to lunar latitudes (the difference can amount to $\sim 1.5°$). The length of a single-color horizontal section in each diagram in Figs 13a–c characterizes the concentration of particles at the corresponding height h with particle sizes in the corresponding range indicated on each graph. The total length of the horizontal section on the diagram corresponds to the total concentration of particles with the indicated size. Figure 13d shows the results of calculations of the maximum possible heights of lofting of dust particles of various sizes for different θ angles. The abundance of sufficiently small particles (with sizes less than 60 nm) depends on the height nonmonotonically, because the behavior of such particles is dynamical (i.e., they do not levitate but move along nearly ballistic trajectories), the time spent by particles of different sizes at the same height is different and, in addition, each horizontal section in Fig. 13, corresponding to a certain range of particle sizes, characterizes a variety of particles. Reducing the size ranges that define the horizontal section results in decreasing the degree of nonmonotonicity in particle abundance.

In general, over the illuminated part of the Moon, for angles θ not very close to 90° (i.e., for not too small values of $\cos\theta$), the distributions of dust particles lofting above the Moon due to electrostatic interactions are similar to those shown in Fig. 13 and are determined by a factor of the order of $\cos\theta$. The main carriers of negative charges in the near-surface layer over the illuminated side are photoelectrons (n_{ph}) and, in some cases, solar wind electrons (n_{sw}), with their concentrations usually related as $n_{ph} \gg n_{sw}$; the positive-charge carriers are dust particles and solar wind protons. Hence, the characteristic size a and concentration n_d of charged dust particles in the near-surface layer of the illuminated part of the Moon can be respectively estimated as characteristic values of the order of 100 nm and 10^3 cm^{-3}. Such a high concentration of dust arises due to a significant concentration of photoelectrons above the Moon (including those knocked out by solar radiation photons from the surfaces of dust particles hovering above the Moon). Over

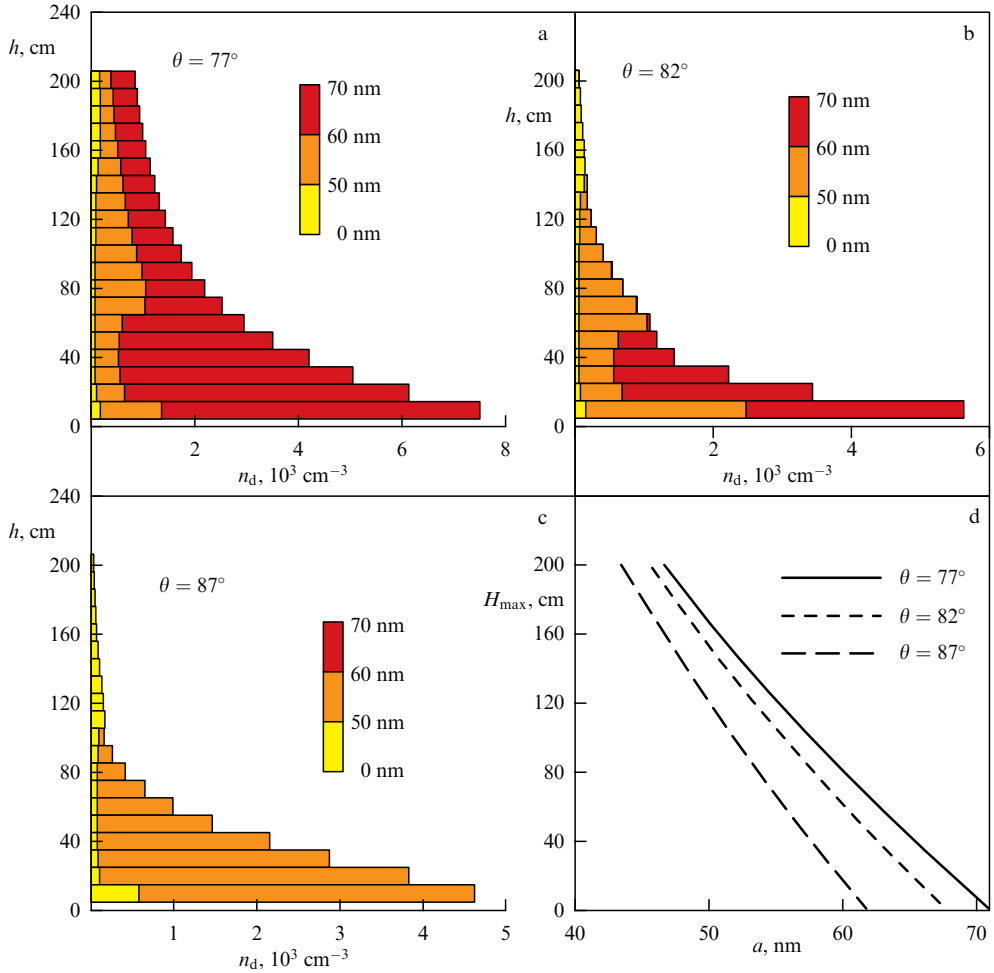

Figure 13. Distributions of dust particles over surface of the Moon for angle θ between local normal and direction to the Sun given by (a) 77°, (b) 82°, and (c) 87°, and (d) maximum possible height of ascent of dust particles [73].

the night part of the Moon, in the absence of photoelectrons, the concentration of charged dust particles with a size of the order of 100 nm can be estimated as $n_d \sim 10^{-2} - 10^{-1}$ cm^{-3}.

We note that, in those areas of the Moon affected by solar wind plasma flows (or magnetospheric plasma when crossing the geomagnetic tail), plasma instabilities can develop, leading to the excitation of Langmuir and electromagnetic high-frequency waves [102, 148]. It was shown in [149] that dust sound waves can propagate in the vicinity of the lunar terminator. Studying wave processes in the near-surface plasma–dust exosphere of the Moon is important from a practical standpoint, because all these plasma instabilities can, among other things, affect the results of measurements of the parameters of near-surface plasma in the course of field studies.

3.3.3 Dust clouds at high altitudes. The plasma–dust exosphere near the lunar surface, as discussed above in this section, forms as a result of the impact of electromagnetic solar radiation and/or flows of interplanetary plasma on the regolith. As already noted, such processes occur on the surface of the regolith, whose thickness is of the order of the Debye radius, in the near-surface plasma–dust layer about a meter in thickness on the illuminated side of the Moon.

A different picture arises when the regolith is exposed to high-speed micrometeoroids of cometary or asteroid origin. The speed of such particles with sizes from 10 nm to 1 mm can reach several tens of km s^{-1} [22]. As shown in Section 2.1, their impact is explosive. Most ejecta (secondary) particles have an initial velocity below the escape velocity from the Moon and return to the surface via ballistic orbits. Micron- and submicron-size secondary particles that are ejected at a near-escape velocity form a highly variable but persistent dust cloud around the Moon. This dust cloud was discovered in lunar orbit by the LDEX (Lunar Dust EXplorer) instrument installed on the lunar orbital satellite LADEE (Lunar Atmosphere and Dust Environment Explorer) [25].

The LDEX instrument was an impact ionization dust detector that measured both positive and negative charges of particles in the plasma cloud that forms when a dust particle hits a target. Measured fluxes of dust particles in lunar orbits at altitudes ranging from 3 to 250 km indicate that the Moon is surrounded by a persistent but highly variable dust exosphere. Based on measurements with the LDEX instrument [150], a model configuration of the dust cloud over the Moon has been proposed (Fig. 14).

3.4 Near-surface electric and magnetic fields

Currently, it is generally accepted that the most likely cause of dust particles detaching from the surface and levitating over the illuminated part of atmosphereless bodies is the electrostatic mechanism [5]. For the Moon, the concept of such a

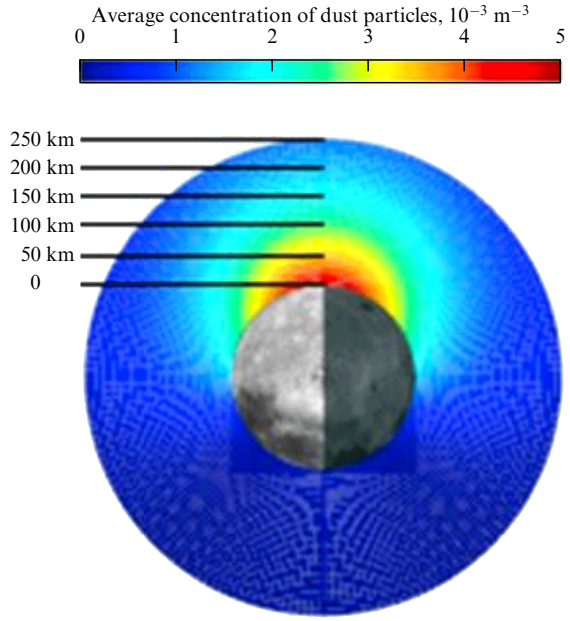

Figure 14. A model year-averaged distribution of lunar dust concentration for particles > 0.3 μm in size, obtained from measurements with the LDEX instrument [150]. The Sun is to the left of the image, and the Moon's orbital motion direction is upward.

process was proposed in [1, 151]. Dust particles located on the regolith surface that have acquired an electric charge q experience the Coulomb force $F_c = qE_c$, the gravitational force $F_g = mg_L$ (where m is the particle mass and g_L is the acceleration of gravity on the Moon), and the van der Waals adhesion force F_a. If the Coulomb force directed upward exceeds the sum of the forces holding the dust grain on the surface, $F_c > F_g + F_a$, the particle detaches from the surface and the van der Waals force disappears. As a result, in the case $F_c \gg F_g$, the particle is accelerated and is pushed away from the surface (lofting). If the electrostatic and gravitational forces acting on a particle are balanced, $F_c \approx F_g$, the particle levitates in the near-surface electric field E_c.

However, two significant problems arise with this mechanism. The first is to understand how a dust grain lying on a surface can accumulate the electrical charge necessary to levitate in the field of the electric double sheet. The second is to elucidate the nature of the force that is capable of detaching a dust grain from the surface, overcoming the van der Waals adhesion force F_{vdW} and the gravitational force F_g. The solution to these problems was considered in several studies, including [6, 9, 152–155].

When considering the detachment of dust particles from a nonconducting surface, an important point is to take the adhesive van der Waals forces F_{vdW} into account; they adhere microparticles to each other or attach them directly to a nonconducting surface. For micron and submicron particles, these forces can be quite significant [152]. For relatively large dust particles (with a characteristic size $R \sim 1$ mm), the adhesion forces $F_{vdW} \propto R$ become insignificant compared with the gravitational force $F_g \propto R^3$ [6]. Therefore, in discussing the particle detachment problem, we first briefly consider methods for assessing the adhesion force.

The magnitude of adhesion forces is usually estimated using the Hamaker model [156]. The parameters of the model are the characteristic sizes R_1 and R_2 of interacting particles, the distance D between their surfaces, and a parameter A introduced by Hamaker. This parameter has the dimension of energy and depends on the properties of the material of the microparticles, but is independent of their shape. Expressions for the magnitude of the adhesion force between two dust particles used by different authors do not differ much [157]. For example, the formula used in [152] is

$$F_{vdW}(D) = \frac{A}{6D^2}\,\frac{R_1 R_2}{R_1 + R_2}\,, \tag{5}$$

with the Hamaker parameter $A \sim 10^{-19}$ J [156]. The distance D between the dust particle surfaces is a rather uncertain quantity. According to [152], D can range from 0.3 nm to 100 nm, depending on the shape and roughness of the dust particles. Taking the characteristic size of microparticles $R \sim 1$ μm, we can estimate the adhesion force F_{vdW} to be in the range from 10^{-7} to 10^{-12} N, which is several orders of magnitude greater than the force of gravity F_g acting on micron-size particles. Thus, to detach a particle with the charge $q = ne$ from the surface, even if the adhesion force F_{vdW} has a minimum value of $\sim 10^{-12}$ N, the electric field strength E above the surface must satisfy the condition

$$\frac{F}{e} = nE \geqslant 10^7 \text{ V m}^{-1}\,. \tag{6}$$

If we again use the value $E \sim 10$ V m^{-1}, then, for a micron-size particle to detach from the regolith surface, its charge must be millions of e, which does not seem realistic. Therefore, it should be assumed that either an extremely strong local electric field exists directly above the surface at the moment of dust grain detachment or dust detaches under the influence of certain forces of a different nature (for example, meteorite impacts or moonquakes).

3.4.1 Charge of a solitary dust grain and a grain of dust lying on the surface. The charge acquired by dust grains lying on the surface and floating above it differ by several orders of magnitude. To understand the cause, it suffices to consider two main mechanisms for acquiring charge: collisions with ions and electrons of the solar wind and the photoelectric effect. In both cases, the process starts with the accumulation of charge on the initially neutral surface of a dust particle. In plasma, this happens because the thermal velocities of electrons are tens of times higher than the thermal velocities of ions (protons in the vast majority of cases in the solar wind plasma). Because the concentrations of electrons and protons are approximately equal, electrons collide with dust grains much more frequently than protons do. As a result, a negative charge accumulates on the surface that absorbs most of the particles incident on it. If photons hit the surface, then positively charged holes appear on it as a result of the photoelectric effect.

Naturally, the process of charge accumulation cannot continue indefinitely. If the surface of the regolith is exposed to plasma, the greater the negative charge of a dust grain on the surface, the more strongly the dust grain repels the incident electrons and attracts protons. Under the photoelectric effect, the greater the positive charge, the smaller the fraction of photoelectrons (the fastest ones) that can escape, while the rest return. The equilibrium value of the charge of a dust grain is attained when the average value of the current flowing onto its surface vanishes.

It is natural to call a dust grain solitary if the field of any other charges is negligibly small in its vicinity. Then, the

currents flowing onto its surface should equalize only under the effect of its own field, which can be considered the field of a point charge. If a grain of dust lies on a plane that is charged uniformly on average, then the field above it is the sum of the fields created both by itself and by all neighboring charges. The strength of such a field is constant in the half-space above the surface and is practically independent of the dust particle's own charge. Therefore, currents flowing to the surface of a solitary dust grain equalize the field that is proportional to its own charge, and currents flowing onto a dust grain on the surface equalize the field acting at any other point on the surface.

Due to external influence, a solitary dust grain could easily acquire a charge $q_0(r)$ sufficient for levitating (but not for detaching from the surface) [158]. The value of q_0 depends on the dust grain radius r and its surface potential $\varphi_0 < 0$ at which the overwhelming majority of electrons flying towards the dust grain are pushed back, equalizing the electron and proton currents. In equilibrium, therefore, $e\varphi_0$ is of the order of the thermal energy of electrons $k_B T_e$, and the charge density on the surface of a solitary dust grain is inversely proportional to r:

$$\sigma(r) = \frac{q_0}{4\pi r^2} = \frac{\varepsilon_0 \varphi_0}{r} \approx -\frac{\varepsilon_0 k_B T_e}{er} \approx -1.5 \frac{10^{-10}}{r} \frac{\text{C}}{\text{m}^2} \approx \frac{10^9}{r} \frac{e}{\text{m}^2} . \quad (7)$$

Here, we set $k_B T_e \approx 15$ eV; a dust grain with a radius of 1 μm can then accumulate about 1000 excess electrons.

A similar situation arises if the charge appears on a solitary dust grain due to photoemission. This time, the charge of the dust particle is positive, and it increases until almost all of the emitted photoelectrons return. For this, $e\varphi_0$ must be of the order of their kinetic energy at the instant they lift off from the surface, and we therefore again arrive at formula (7), where we replace the thermal energy with the difference between the energy of a light quantum and the work function. As a result, the sign changes and the value of σ slightly decreases, but in any case we have hundreds of excess elementary charges e on the surface of a micron-size dust particle.

For small-radius solitary particles, a high surface charge density is necessary, because the electric field they create practically vanishes already at a distance h of the order of ten of its radii r. Therefore, the potential difference must be equal to $\varphi_0 \propto E_0 h$ in this layer, where $E_0 = \sigma/\varepsilon_0$ is the field strength above the surface. That is why the surface charge density of a solitary grain should increase rapidly as its radius decreases.

An entirely different situation occurs when a dust grain lies on a flat surface. In that case, the average current onto the surface is zero due to the deceleration of electrons inside the near-surface layer, above which the field, equal to $E_0 = \sigma_0 \varepsilon_0^{-1}$ immediately above the surface, is screened. In plasma physics, such a layer is called a plasma sheath, and its thickness near the Moon is of the order of the Debye screening radius $r_D \sim 1$ m [5]. Under the photoelectric effect, the plasma sheath (in this case, a layer of photoelectrons lifting off and falling back) screens the positive surface charge, and the field above the layer is zero. More specifically, if the field strength above the surface is about 10 V m^{-1} and the photoelectron energy does not exceed 10 eV, then the thickness of the photoelectron layer is also about a meter. Thus, in equilibrium, the charge density on a flat surface σ_0 is in any case r_D/r times less than on the surface of a radius-r dust grain, and if such a dust grain lies on the surface, then only the charge $\pi\sigma_0 r^2$ accumulates on it (see the comparison of two models for a dust grain charge in [152]). The Coulomb force acting on it is then equal to

$$F_C \approx 2\pi r^2 \varepsilon_0 E_0^2 , \quad E_0 = \frac{\sigma_0}{2\varepsilon_0} . \quad (8)$$

Therefore, for $E \approx 10$ V m^{-1} [123], the Coulomb force acting on a dust grain with $d \approx 1$ μm should be about 10^{-21} N, which is a billionth of the lower limit estimates for F_{vdW}. Moreover, with an average charge density on the illuminated surface $\sigma_0 \approx \varepsilon_0 E \approx 10^{-10}$ C m^{-2}, which corresponds to the field strength $E \approx 10$ V m^{-1} above the illuminated surface of the Moon, only one in a thousand dust grains 1 μm in diameter would have an excess charge of at least $1e$.

Nevertheless, dust levitates above the surface of the Moon and other atmosphereless bodies. It is this kind of dust that is responsible for the repeatedly observed near-surface LHG. The presence of dust above the surface has also been repeatedly confirmed by instruments aboard lunar probes (see Section 2.3) and in laboratory experiments (see, e.g., [6, 13, 152, 159, 160]). It is to be assumed that dust most likely takes off and levitates under the influence of Coulomb forces, and options for resolving this paradox appeared only recently.

3.4.2 Microparticle charge fluctuations on the surface [155]. Charges $+e$ appear on the illuminated surface of the Moon due to the photoelectric effect. The surface becomes positively charged, and photoelectrons return to it, bringing the negative charge $-e$ to a random location on the surface. In general, according to measurement data, the surface is charged positively, and an electric field with the strength $E = 10$ V m^{-1} exists above it [123]. The density of the surface charge creating this field is $\sigma_0 \approx 2\varepsilon_0 E \approx 10^9 e$ m^{-2} $\approx$ $10^{-3} e$ μm^{-2}, and the photocurrent density from the surface is $j_{ph} \approx 40$ μA m^{-2} $\approx 250e$ μm^{-2} s^{-1} [122]. Thus, the sum of the *moduli* of charges incident in 1 second on any area on the surface of the Moon is hundreds of thousands of times greater that the *average* value of its charge. In such a situation, fluctuations inevitably arise, and the amplitude of these fluctuations depends sharply on the size of the area under observation.

If we let $n_\pm(t)$ denote the number of charges of the corresponding sign that appeared in an area ΔS during the time interval from t to $t + \mathrm{d}t$, then the current density approaching this area is

$$j(t) = j_+(t) + j_-(t) , \quad j_\pm(t) = \pm \frac{e n_\pm(t)}{\Delta S \, \mathrm{d}t} . \quad (9)$$

If we define the average value of the current density as the sum of its values at different times $t_1, t_2, \ldots, t_K$, with $K \gg 1$, divided by K, then $\langle j_\pm \rangle = \pm j_0$ and $\langle j \rangle = 0$ in the stationary state. Here, j_0 is the *average* value of the density moduli of the positive- and negative-charge currents to the surface, which are equal to each other in a stationary state. However, these currents are stochastic in nature, and therefore their instantaneous values fluctuate. This means that more positive charges fall on the selected area ΔS at some instants, and more negative charges at others. Therefore, the instantaneous value of the charge accumulated in this area,

$$q(t) = \int_0^t j(t') \, \mathrm{d}t' , \quad (10)$$

also fluctuates, although its average value vanishes:

$$\lim_{t\to\infty}\frac{q(t)}{t}=0\,.$$

Because the probabilities of protons and electrons hitting the region ΔS are the same in a stationary state, the process under consideration is quite similar to a series of coin tosses. If heads and tails are denoted by ±1, then the result of a series of N tosses is a sequence of N numbers like $+1,+1,-1,\ldots,-1$. Most probably, in any series of N tosses, heads and tails would appear an unequal number of times, i.e., the sum of all ±1 would be some positive or negative number $\pm v$ (cf. Eqn (10)). If we perform many series of N tosses and average their results, we obtain $\langle v\rangle=0$, but if we average not v, but v^2, then

$$\langle v^2\rangle=\left\langle(+1,-1,\ldots,-1)^2\right\rangle\equiv N\,. \tag{11}$$

Because the average *square* of the excess number of heads or tails is N, the amplitude of accumulated charge fluctuations is $\delta q=ve$, and because $N=2e^{-1}j_0\Delta St$, we have

$$\langle\delta q\rangle\approx\sqrt{2ej_0\Delta St}\,. \tag{12}$$

In such a situation, on a microscale, the surface should look like a set of chaotically scattered 'charge spots' of different sizes, with different positive or negative charges. For a noticeable field to be created above the surface, it must carry a certain average charge in a macroscopic sense, and therefore the number or the average charge of same-sign spots (positive on the illuminated lunar surface) must prevail, and hence the average density over the entire surface charge must be $\sigma_{0\pm}\neq0$.

The distribution of charge spots over the surface is not static; their shapes and sizes, as well as charge magnitudes and signs, fluctuate. At each instant t, the increment $\delta x(t)$ of any fluctuating quantity $x(t)$ is determined by the competition of two contributions: stochastic processes (Brownian walk) and a unidirectional process that tends to suppress any deviation of x from its stationary average value x_0 (damping). If the charged particles and light quanta hit the surface totally randomly, then according to (12) the amplitude of charge fluctuations in the spots should increase over time in proportion to $\sqrt{t}$. Because the amplitude of the charge density fluctuations on the surface of an emerging spot increases, the amplitude of fluctuations of the field strength above it also increases,

$$\langle\delta\sigma\rangle\approx\langle\delta q\rangle\Delta S^{-1}\propto\Delta S^{-1/2}\,,\quad\langle\delta E\rangle\approx(1/2)\varepsilon_0^{-1}\langle\delta\sigma\rangle\,, \tag{13}$$

and hence both these amplitudes are inversely proportional to the linear size of the spot.

Without a doubt, however, the amplitude of fluctuations cannot increase indefinitely over time: because of the excess charge δq appearing on an area ΔS, the incidence of new ions and electrons onto it would no longer be random. Ions with a charge of the same sign as δq would be repelled from ΔS and hit it less often, and ions with an opposite-sign charge would hit the area more often. This is exactly how the mechanism of constant suppression of the resulting fluctuation works in this case, determining the fluctuation lifetime τ. Immediately after its occurrence, the fluctuation amplitude increases in proportion to $\sqrt{t}$, and the damping processes at small amplitudes are not very significant. But as t increases, the rate of increase in amplitude, proportional to $t^{-1/2}$, decreases, attenuation processes come to the fore, and, having existed for a period of time of the order of τ, the fluctuation disappears. Based on these considerations, we can expect that the amplitude of charge fluctuations in equilibrium is approximately equal to the maximum value attained by $\langle\delta q\rangle$ in (12) during the time τ:

$$\langle\delta q\rangle_{\rm eq}\approx\sqrt{2ej_0\Delta S\tau}\,. \tag{14}$$

In general, this conclusion does not contradict the results obtained by solving equations for stochastic processes, which is quite natural. We do not discuss various versions of such equations here, which are quite well known and have been described in detail in textbooks. However, we briefly discuss a specific problem that arises when trying to apply these equations to describing charge fluctuations on a flat surface.

As is clear from Eqn (14), the central problem in studying surface charge fluctuations is to calculate τ. Because the rate of decay of a fluctuation is determined by the field above it, the primary problem in calculating τ is to find the potential or field strength above the surface on which charge fluctuations occur. As was mentioned above when discussing the charge of a solitary particle, only the field of the particle's own charge controls the current flowing to its surface, i.e., the rate of change of the charge over time. Because the field above a solitary particle is directly proportional to its charge, describing charge fluctuations in such a system requires solving standard equations with one fluctuating variable.

In the case of fluctuations of a charge spot on a plane, the rate of change of its charge is also controlled by the field above it. However, this field is now created not only by the charge of the spot but also by all charges located on the plane,

$$\begin{aligned}&\mathbf{E}(\mathbf{R})=\frac{\sigma_0}{2\varepsilon_0}\,\hat{e}_z+\int_S\frac{\sigma(\mathbf{r})-\sigma_0}{4\pi\varepsilon_0|\mathbf{R}-\mathbf{r}|^3}\,(\mathbf{R}-\mathbf{r})\,\mathrm{d}S\,,\\&\mathbf{R}=(x,y,z)\,,\quad\mathbf{r}=(x,y)\,,\end{aligned} \tag{15}$$

where σ_0 is the average value of the charge density on the plane and $\hat{e}_z$ is the unit vector along the z-axis perpendicular to the plane. Thus, the rate of change of any charge spot depends on all charge spots on the plane, and we therefore have a system of infinitely many elements fluctuating and interacting with each other.

In reality, the problem is even more complicated because, in addition to the field of charge spots, the field of space charges above the surface (plasma sheath and/or the layer of photoelectrons) must be taken into account. Still, neglecting the contribution of the space charge, we can find the potential φ from the Poisson equation

$$\Delta\varphi(\mathbf{R})=-\varepsilon_0^{-1}\left[\sigma_0+\delta\sigma(\mathbf{r})\right]\delta(z)\,,\quad\delta\sigma(\mathbf{r})=\sigma(\mathbf{r})-\sigma_0\,, \tag{16}$$

which can be solved analytically [161]. Here, $\delta(z)$ is the delta function; expanding the inhomogeneous addition to the surface charge density in a series $\delta\sigma(\mathbf{r})=\sum_{\mathbf{k}}\delta\sigma_{\mathbf{k}}\exp(\mathrm{i}\mathbf{kr})$, we can obtain an *exact* solution of this equation for each Fourier component:

$$\delta\varphi(\mathbf{R})=\delta\varphi_{\mathbf{k}}\exp\left(\mathrm{i}\mathbf{kr}-k|z|\right)\,,\quad\delta\varphi_{\mathbf{k}}=\frac{\delta\sigma_{\mathbf{k}}}{2\varepsilon_0 k}\,. \tag{17}$$

As a result, the problem of fluctuating local charge spots interacting with each other reduces to the *exactly* solvable

problem of an ensemble of charge waves fluctuating independently of each other.

It is clear from (17) that, when charge spots fluctuate on the surface, a thin layer of a pulsating electric field appears above it. It can be imagined as a superposition of fields fluctuating independently of each other, each of which has a periodic structure with its own wave vector **k** parallel to the xy plane, but at the same time very rapidly attenuates, as $\exp(-k|z|)$, with distance from the plane. Consequently, the shorter the wavelength $\lambda = 2\pi k^{-1}$ of the resulting periodic structure, the faster its field decays with distance from the surface. In addition, it follows from (16) that the smaller λ, the weaker the field created by this charge density wave, and therefore the longer its relaxation time, i.e., the smaller the size of the charge spot and the longer its lifetime. We emphasize that such a conclusion was obtained in [161] in the case where the current density onto the charge spot is proportional to the potential on its surface. Apparently, other factors must also be taken into account (e.g., the usual electrical conductivity $j \propto E$) when calculating the current, which can make the relation between the size of the charge spot and its lifetime more complex.

In conclusion, we note that, as a result of fluctuations in the charge of a microparticle lying on the surface of the regolith, the local electric field strength E immediately above the surface of charge spots with a size of the order of a micron can be $\sim 10^6 - 10^7$ V m^{-1} [155, 161]. The authors of [162], who conducted experiments with quantum dots embedded in the surface on which charge fluctuations occurred, arrived at the same conclusion. When substituting the above values of E in (8), it becomes clear that the Coulomb force acting on a dust grain lying near the center of such a spot can easily exceed at least the lower bound of the estimated adhesion forces.

3.4.3 Other mechanisms for emergence of strong local fields. A different approach to explaining the emergence of a strong electric field near the surface of the Moon was considered in [9], where a model was proposed for the emergence of a local electric field near natural inhomogeneities of the lunar surface (craters, rocks, and so on). The model was developed in the cases where the zenith angle of the Sun is close to 90°, which is most typical for the terminator and polar regions. It was shown that, if the characteristic size of a regolith irregularity is much smaller than the local Debye radius, then, given the low conductivity of the regolith, a sufficiently strong electric field can arise under the influence of external factors at the boundary of light and shadow, and this field can ensure the detachment of dust grains from the surface and their levitation.

A more sophisticated model explaining how a sharp increase in the charges of dust particles can occur was proposed in [154], where it was noted that light quanta or fast particles can penetrate through the gaps between dust particles of the uppermost regolith layer into natural subsurface caverns and knock out electrons from the underlying layer of particles. The knocked-out electrons can be absorbed by dust particles in the upper layer of such a cavern. A diagram of the proposed mechanism, called the patched charge model by the authors, is presented in Fig. 15. In this figure, dust particles shown with gray spheres form a microcavity (in the center of the figure). Photons and/or electrons and ions hit the surfaces of dust particles (shown in blue) and charge them, giving rise to the emission of photoelectrons or secondary electrons. Some of the emitted

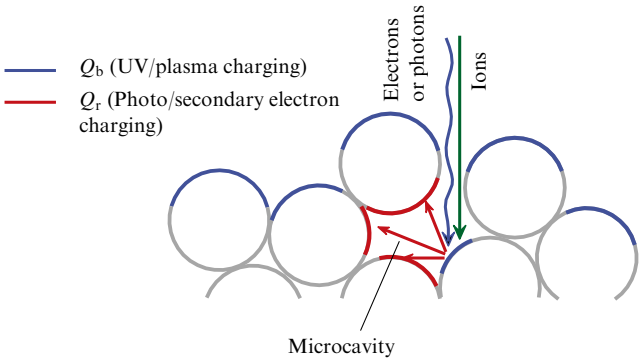

Figure 15. Patched charge model [154]. Dust particles (gray spheres) form a microcavity (in the center). Photons and/or electrons and ions hit dust particle surfaces (marked in blue) and charge them, and photoelectrons or secondary electrons are then emitted. Some emitted electrons are reabsorbed by dust particles inside the cavity (red areas on the surface of dust particles), which then acquire a negative charge.

electrons are reabsorbed by dust particles inside the cavity (red areas on the surface of dust particles), and these then become negatively charged.

According to the authors, when the negative charges of dust particles on the ceiling of the cavity become sufficiently large, the Coulomb repulsion force between negatively charged particles causes them to detach from the surface and fly up. We note that this model is currently quite widely used by some researchers.

3.4.4 Temperature dependence of conditions for detachment of particles. When considering the problem of detachment of microparticles from the surface, it should be borne in mind that, if the magnitude of the adhesion forces is several piconewtons, then the detachment probability must strongly depend on temperature. Indeed, van der Waals forces decrease quite rapidly with distance D between particles, $F_{\rm vdW} \sim D^{-2}$ (see Eqn (5)). Therefore, the work required to detach particles initially located at a distance D is

$$W = F(D)\, D \int_1^\infty \frac{{\rm d}x}{x^2} = F(D)D\,, \tag{18}$$

which turns out to be not too big. With the values $A \sim 10^{-19}$ J and $D \sim 0.3$ nm [152], it follows that, for characteristic particle sizes $R_1 \approx R_2 \approx 0.5$ μm, the adhesion force is $F_{\rm vdW} \sim 5 \times 10^4$ pN and $W \approx 1.5 \times 10^{-17}$ J, which corresponds to the thermal energy $k_{\rm B}T$ at $T \approx 10^6$ K. If $D \approx 100$ nm, then $F \approx 0.4$ pN, $W \approx 4 \times 10^{-20}$ J, and $T = W/k_{\rm B} \approx 3000$ K. This case corresponds to the standard estimate of the dipole bond energy $W \approx 10$–20 kJ mol^{-1} [163]. This means that, at $T \approx 400$ K, i.e., close to the temperature of the lunar surface illuminated by the Sun [76], approximately three out of every 10,000 dust grains lying on the surface have the energy sufficient to take off due to thermal fluctuations. Moreover, under such conditions, solely due to such fluctuations, the smallest dust grains with $d \sim 10$ nm can levitate at a height of about 1 m [164].

In addition, when analyzing the destructive effects of lunar dust, we must take the rotation of dust grains into account: when detached from the regolith surface, they acquire some angular momentum. Due to the principle of the equidistribution of energy over the degrees of freedom, a

spheroid of mass m should rotate with the equatorial speed $v \approx \sqrt{5k_B T/2m}$. For a micron-size particle (weighing $\sim 10^{-15}$ kg), this speed is of the order of millimeters per second, and for a grain of dust with a diameter of 10 nm (weighing $\sim 10^{-21}$ kg), it is already several meters per second. As noted in [164], this means that, above the regolith surface, levitating and rotating dust grains with a characteristic size of tens of nanometers can make tens or even hundreds of millions of revolutions per second. This property of levitating dust particles can qualitatively change the degree to which they impact an obstacle (this problem is discussed in Section 4).

3.4.5 Near-surface magnetic fields. Measurements with magnetometers at the Apollo landing sites (on the visible side of the Moon) showed that the magnetic field strength on the surface is in the range of $\sim 10^{-3}-10^{-4}$ G [165]. Measurements and global mapping of magnetic fields from lunar orbits by the Lunar Prospector [166] and Kaguya [167] spacecraft revealed that there are areas of local magnetization on the Moon, called magnetic anomalies. The magnetic field strength in zones of magnetic anomalies can reach 100 nT (10^{-3} G) [166]. It was suggested in [79] that magnetic anomalies can create mini-magnetospheres, as a result of which solar wind fluxes can be deflected over areas of magnetic anomalies. According to observations by Lunar Prospector [168] and Chandrayaan-1 [169, 170], local magnetic anomalies are associated with mini-magnetospheres. Mini-magnetospheres have features characteristic of normal planetary magnetospheres, namely, a collisionless bow shock [171]. The electric field associated with the small-scale (of the order of several hundred kilometers) collisionless bow shock is responsible for deflecting the solar wind around the mini-magnetosphere, its shape being determined by the shape of the collisionless bow shock — a classical phenomenon in plasma physics, widespread in many space and astrophysical processes, e.g., when the plasma flow of the solar wind interacts with a magnetized planet [172].

Numerical modeling of the interaction of solar-wind particles with magnetized areas on the lunar surface shows that a dipole buried 100 km below the surface with a field strength of 50 nT at the surface and 10 nT at an altitude of 100 km above the surface deflects the solar wind flow and causes the formation of a bow shock and magnetopause [173]. However, the bow shock and the magnetopause are not clearly separated in the simulation because of the small size of the mini-magnetospheres. The spatial size of magnetic anomalies (about 100 km) is comparable to the ion gyroradius of the solar wind (usually 30–150 km) and, as noted in [169], kinetic effects must be important under this condition. Figure 16 illustrates the interaction of the solar wind with the magnetic field of the lunar crust as observed by the Lunar Prospector orbiter [79].

An important consequence of the formation of a mini-magnetosphere is that it protects the regolith surface from the incoming flow of ions by shielding the surface of the Moon from the solar wind, and hence the action of the solar wind on the regolith changes in the mini-magnetosphere areas. Apparently, this fact is related to the so-called 'lunar swirls,' which in many cases are associated with lunar magnetic anomalies and high-albedo areas of the lunar surface. Analyses of the spectra obtained using UV and IR cameras installed on the Clementine lunar orbiter showed that, in the studied areas of the lunar surface where lunar swirls were observed, external impacts caused less erosion of the regolith,

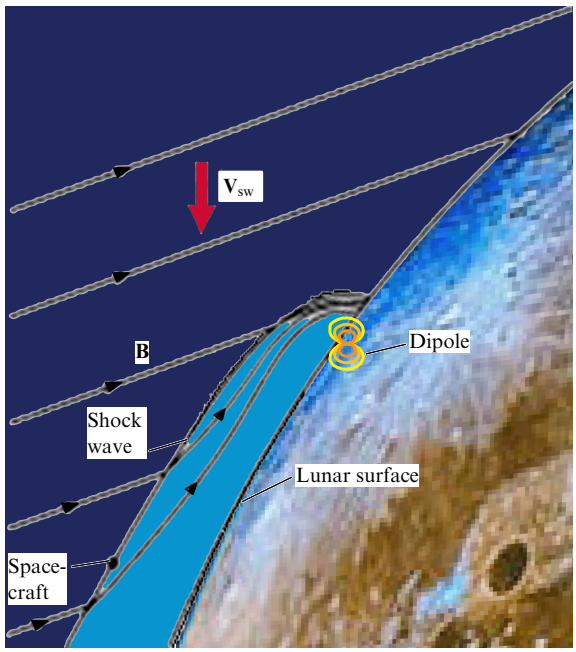

Figure 16. Interaction of solar wind with the magnetic field of lunar crust. This magnetic field is represented by a dipole placed at the focal point of the surface of a hyperbolic shock wave crossing the Lunar Prospector spacecraft. Also shown are interplanetary magnetic field lines **B** and solar wind velocity vector $\mathbf{V}_{sw}$ [79].

while the areas immediately adjacent to them experienced increased weathering [174, 175]. Lunar regolith microparticles can be transported along the surface by weak electrical fluctuations created by the interaction of the solar wind with magnetic anomalies over distances comparable to the length of the emerging swirl [176].

For approximately a quarter of its orbit, the Moon is located in the tail of Earth's magnetosphere, where the magnetic induction of typical magnetic fields is of the order of 1 to 10 nT [177]. The Moon moves in orbit at a speed of about 1 km s^{-1}. Because the dust plasma of the Moon is 'attached' to its surface, this results in charged dust particles moving relative to the magnetic field lines of the geomagnetic tail with a speed of the order of 1 km s^{-1}. Therefore, despite very small values of the magnetic field induction near the Moon, a rather noticeable magnetic component of the Lorentz force acting on dust particles is feasible due to the rather large relative velocity. The motion of the Moon in the tail of Earth's magnetosphere, the magnetic field induction vector **B**, the speed of a dust particle $\mathbf{V}_d$, and the magnetic component of the Lorentz force F_L are schematically shown in Fig. 17.

Due to the action of these magnetic fields during the passage of the Moon through the tail of Earth's magnetosphere, meridional (from $-90°$ to $90°$) transport of charged dust particles over the lunar surface is possible over long distances [178]. The transfer of dust particles from the latitudes adjacent to the lunar poles to the equator of the Moon due to the uncompensated magnetic component of the Lorentz force is a fundamentally important, qualitatively new effect, absent outside the region of the magnetospheric tail. We note that the transfer of dust particles is accompanied, in particular, by changes in their charges, because the number of photoelectrons surrounding a dust particle and affecting its

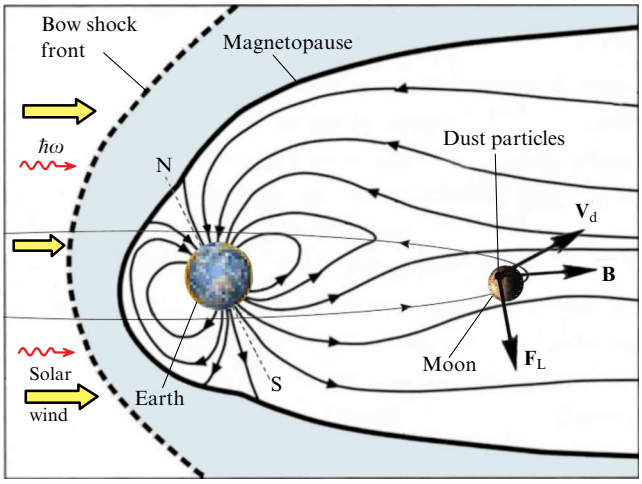

Figure 17. Schematic of motion of the Moon in the tail of Earth's magnetosphere. Lunar orbit is shown with a thin line; arrows on lunar orbit show the Moon's motion direction. Solar wind and solar radiation photons ($\hbar\omega$) are also depicted [178].

charge depends on the angle between the local normal to the surface and the direction to the Sun. In addition, the charge of a dust particle is also affected by the height at which it is located. This height can change during the transfer process. The magnetic part of the Lorentz force acting on dust particles located in areas of magnetic anomalies is either smaller than or comparable to a similar force calculated for the magnetic fields of Earth's magnetotail in the orbit of the Moon. However, due to the strong localization of areas of magnetic anomalies, their influence on the dynamics of charged dust particles above the Moon does not lead to similar qualitative effects.

4. 'Toxicity' of lunar dust

Of all the known features of the lunar environment, the most unexpected and apparently the most mysterious one is lunar dust. Although the USA Apollo crewed program carried out from 1969 to 1972 was assessed as amazingly successful [179], American astronauts were faced with an unforeseen and very unpleasant problem: the aggressive effects of lunar dust. The crews of each of the six Apollo missions to the lunar surface noted insurmountable problems caused by exposure to lunar dust. Each subsequent Apollo mission attempted to account for the effects of dust, but no solution was found to minimize its impact. Gene Cernan, the commander of the last mission, Apollo 17, expressed his reaction to the impact of lunar dust most succinctly. In his report, he wrote: "I think dust is probably one of our greatest inhibitors to a nominal operation on the Moon. I think we can overcome other physiological or physical or mechanical problems except dust" [17].

4.1 Exposure to natural lunar environment

Even at the early stages of lunar exploration, several reflective systems for laser ranging were deployed on the lunar surface. Laser reflectors were installed on Lunokhod-2 [130] and by American astronauts at the landing sites of the Apollo missions [180]. During the first few months of observations, the signal from the Lunokhod-2 laser reflector was 25 times stronger than that from the Apollo reflectors. However, after almost 40 years of operation of these systems on the lunar surface, the signal magnitude from the Lunokhod-2 reflector became an order of magnitude lower than that of the Apollo [180]. This may be because the reflective surfaces of Lunokhod-2 had greater exposure to external influences than the Apollo reflectors. Such design features may reduce their reflectivity due to deposition of levitating lunar dust and exposure to particles associated with micrometeoroid bombardment. In any case, an analysis of the operation of these systems over several decades showed that, in natural conditions not perturbed by anthropogenic factors, the optical systems performed their functions quite successfully, but the gradual degradation of the optics was recorded on a decade time scale [180].

Another important source of information on the impact of the lunar surface environment on lander systems was the analysis of the long-term stay of the Surveyor 3 robotic lander on the lunar surface. This analysis was made possible because the crewed Apollo 12 descent module landed, as had been planned, in close proximity to the Surveyor 3 landing site. By the time Apollo 12 arrived on the lunar surface (November 24, 1969), the Surveyor 3 lander (lunar landing date April 20, 1967) had been on the lunar surface for more than 2.5 years. The distance between the two landing locations was ~ 83 m [181]. Figure 18 shows a photograph of the Apollo 12 mission commander, astronaut Charles "Pete" Conrad, at the Surveyor 3 robotic lander. The Apollo 12 lunar module can be seen in the background [182].

Some systems and equipment removed from Surveyor 3 were returned to Earth. Based on the results of laboratory studies, a large number of features pertaining to changes in the surface of the lander and its systems were noted. In particular, photoinduced discoloration of surfaces was discovered. Almost all exposed surfaces of the chamber were partially covered with a thin layer of lunar dust. There were noticeable differences in the number and apparent size of dust particles on different surfaces. A detailed analysis revealed that fine-grained particles were implanted on the spacecraft

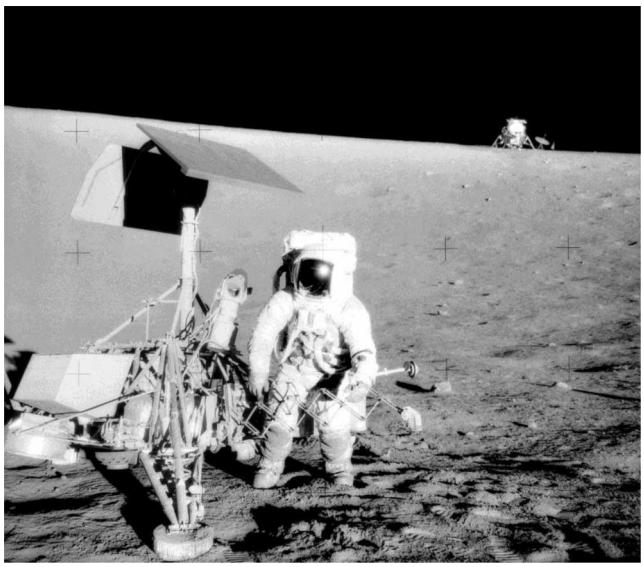

Figure 18. Apollo 12 mission commander Charles "Pete" Conrad at the Surveyor 3 robotic lander. Apollo 12 lunar module can be seen in the background [182] (https://upload.wikimedia.org/wikipedia/commons/4/4e/Surveyor_3-Apollo_12.jpg).

primarily during the initial landing of Surveyor 3, and then during the descent and landing of the Apollo 12 lunar module. The presence of dust, even in very small quantities, can significantly affect temperature control systems and characteristics of equipment on the lunar surface. It was demonstrated that the landing of the Apollo 12 lunar module covered the surface of Surveyor 3 service systems with an additional layer of dust. Analyses of organic contaminants, of micrometeor impacts on the surface of the apparatus, and of radiation damage were also performed.

Nevertheless, the principal conclusion from the analysis of the state of optical systems after long-term (several decades) exposure and the condition of the service systems of the Surveyor 3 lander after more than 2.5 years on the lunar surface is that the impact of the plasma–dust exosphere, and of levitating dust particles in particular, in a natural environment does not have a significant effect on sensitive surfaces and the condition of engineering systems of landing vehicles.

4.2 Aspects of anthropogenic factor

The results of six crewed expeditions of the Apollo program showed that the situation changes significantly when anthropogenic factors influence the regolith and exosphere of the Moon. Such factors include the operation of the engines of descent and ascent stages when landing on and taking off from the surface of the Moon, the motion of astronauts or a rover on the surface of the regolith, and the operation of technological systems (for example, a drilling rig) on the ground. In such cases, in addition to natural processes affecting the dynamics of dust particles, so-called 'collateral dust' arises [183]. Moreover, the transfer of such collateral dust of anthropogenic origin is several orders of magnitude higher than the transfer of natural dust [30]. Collateral dust causes a much greater impact on service systems and on astronaut operations and health than natural dust transfer processes. It has been noted that the effects of collateral dust pose a much greater threat to astronaut safety and mission success [17, 18, 30, 179, 184].

The effects of collateral lunar dust on lander systems and astronaut activities on the lunar surface during the six Apollo lunar missions on the surface were classified into nine categories:

(1) deterioration of visibility when dust rises;
(2) false instrument readings;
(3) dust deposition and surface contamination;
(4) loss of traction with the ground when moving on the ground;
(5) jamming of turnable components of mechanisms;
(6) active erosion of surfaces;
(7) problems with thermal regulation and control systems;
(8) violation of seals and air-tightness of systems;
(9) breathing problems and other factors related to human health [17].

The astronauts first encountered the problem of reduced visibility during landing while the engines of the Apollo 11 lunar module were burning. At an altitude of approximately 30 m above the surface, due to the operation of the descent engines, a cloud of dust arose, which became increasingly dense as the altitude decreased. There was a risk that one of the landing legs would touch a large boulder or fall into a small crater. Therefore, for the landing of the subsequent Apollo 14, 15, and 16 missions on the lunar surface, the landing profile was adjusted. But in those cases, too, difficulties were encountered in inspecting the site before contact with the surface. The visibility problem also had a consequence that the landing speed sensors of the Apollo 12 and 15 vehicles showed false readings due to a cloud of dust that arose during the burn of the landing engines [17].

Moon dust turned out to be extremely abrasive. According to the astronauts, after working outside the lunar module, the instrument dials and sun visors of their helmets were so scratched that it was impossible to discern the instrument readings. The astronauts noted that after eight hours of work on the lunar surface, the spacesuits and gloves, especially after soil drilling, had significant abrasions and, had it become necessary to do one or two additional moonwalks, they could have lost their air-tightness [17]. For example, the space suit of Pete Conrad, the Apollo 12 mission commander, which was airproof before the first EVA from the lunar module, was losing pressure at a rate of ~ 0.01 atm min^{-1} after the first EVA and ~ 0.017 atm min^{-1} after the second EVA. Because a safe leak was 0.02 atm min^{-1}, the safety of a third EVA would have been questionable if it had been planned. Dust that penetrated the moving parts of the pressurized suit led to such great difficulties in movement that another scheduled moonwalk would have been impossible [17]. It was impossible to use the zippers on the spacesuits after working outside the lunar module. The abrasive properties of lunar dust affected not only service systems and the activities of astronauts but also scientific results: in particular, due to exposure to dust, the sealing of all sealed samples of the lunar atmosphere brought to Earth for analysis was broken and, thus, all of them turned out to be useless. It was noted that, during a long-term stay on the Moon, maintaining safe living conditions would require more attention to ensuring the air-tightness of systems and spacesuits and creating more dust-resistant seals.

When astronauts worked on the surface, it turned out that dust quickly covered all surfaces with which it came into contact, including space suits, boots, hand tools, equipment, and lunar module systems. Dust deposition required the astronauts to perform additional work to clean clothing and equipment, but this also turned out to be ineffective. That the attempts to remove dust under lunar conditions were ineffective was in no way expected based on the results of tests on Earth. As a result, the operating temperature of some systems exceeded the nominal one by 20 °C and individual devices of the Apollo 16 and 17 equipment deteriorated their characteristics due to overheating. It is for this reason that John Young, the Apollo 16 commander, noted that ''dust is the number one concern in returning to the Moon.''

However, the most unwanted factor of lunar dust is its effect on human health. For the Russian lunar program, these problems are planned to be studied at the Institute of Medical and Biological Problems of the Russian Academy of Sciences. Here, we only note the reviews of American astronauts about working on the lunar surface. Crew members of the Apollo landers reported that lunar dust microparticles caused irritation to the skin, eyes, and the respiratory system. Moon dust has a pungent odor reminiscent of gunpowder, which is apparently a consequence of the presence of volatile substances on the surface of dust particles. Dust penetrated the astronauts' clothing; when removing their clothes, the astronauts discovered that they were covered in dust. During the return flight, in the absence of gravity, the dust that had been brought into the lunar module rose and spread throughout its volume. The crew breathed this atmosphere

Figure 19. Apollo 17 mission commander Gene Cernan in a dusty spacesuit in the lunar module after an EVA on the lunar surface. Portion of a NASA photo (https://www.smithsonianmag.com/smart-news/eugene-cernan-was-more-just-last-astronaut-moon-180961830/) [18].

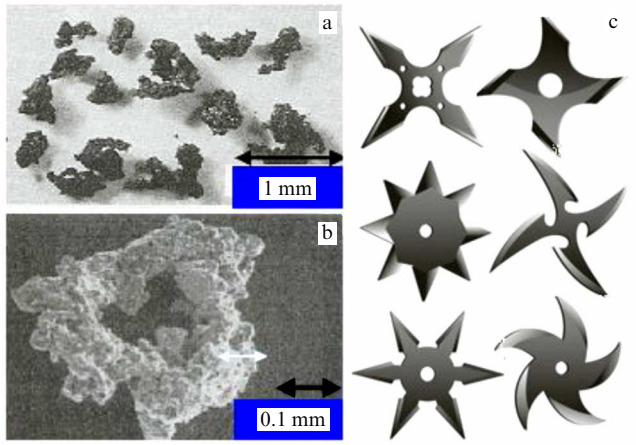

Figure 20. (a, b) Photographs of lunar dust particles taken with a microscope (https://science.nasa.gov/science-news/science-at-nasa/2005/22apr_dontinhale). (c) Examples of images of shuriken (throwing stars) (https://army-today.ru/oruzhie/syuriken).

with dust, which irritated their eyes. The dust removal equipment available on board was ineffective. After the discovery of these features of lunar dust during the first mission, measures were taken to reduce such effects on subsequent flights. However, the toxicity of micron and submicron particles found on space suit material indicates the need for constant monitoring of particle concentrations inside the lunar module and, in the future, in the long-term habitat at lunar exploration stations [184]. Figure 19 shows a photo of Gene Cernan, the Apollo 17 mission commander, in the lunar module wearing a dusty spacesuit after working on the surface of the Moon.

Based on the Apollo experience, it can be concluded that the severity of the dust problem was originally underestimated [179]. When planning the Apollo missions, the properties of the plasma–dust exosphere under natural conditions on the Moon were taken into account, with the dynamics of dust determined by effects due to solar radiation and flows of micrometeorites incident on the regolith surface. Under these conditions, as shown by the results of experiments on robotic landing vehicles, the influence of dust dynamics, although noticeable, did not have a critical impact on the operation of scientific and service equipment. During crewed missions, a radically different degree of influence of dust particles on the service systems of landing vehicles was discovered, associated with anthropogenic activity and human operations on the surface. Collateral dust arising under such dynamical conditions, caused by the mechanical impact of human activity on the regolith surface, is much more dangerous compared to natural dust. As noted in reports on the results of the Apollo missions, the transfer of dust associated with the activities of astronauts on the lunar surface can be orders of magnitude higher than the transfer of dust as a result of natural processes [30]. Therefore, active work on the lunar surface can be very dangerous for astronauts, life support systems, and the service systems of landers and equipment used by astronauts.

The unusual ability of lunar dust to penetrate the seals of airproof systems and stick to various surfaces can be considered from the standpoint of the dynamical properties of particles levitating above the surface. Due to the impact origin of such particles, their shapes are extremely irregular and most of them have sharp edges [70, 74]. As was shown in Section 3.4, dust grains with a characteristic size of tens of nanometers levitating above the surface of the regolith when detached from the surface can acquire angular momentum and rapidly rotate [164]. Such rotating mineral particles, when interacting with an obstacle, are not just 'projectiles,' but can also be a kind of 'cutting tool,' reminiscent of miniature replicas of oriental shuriken (throwing stars or ninja stars), which have great destructive power. Figure 20 shows photographs of microparticles and examples of shuriken.

It is perhaps this feature, in combination with the existing electrostatic charge, that explains the amazing ability of collateral dust arising from anthropogenic impact on the lunar regolith to aggressively affect the surfaces of sensitive instruments and service systems of landers, penetrate through airproof seals, and affect humans, despite their apparent protection from such influence. The experience of the Apollo crewed missions led to the development of a new scientific and practical research area: the development of methods and tools for minimizing the influence of lunar dust (see, e.g., review [185]).

5. Unsolved problems of the dynamics of plasma–dust processes on the Moon

Explorations of the Moon carried out more than 50 years ago, at the dawn of the space age, stimulated intensive analytic and laboratory studies aimed at modeling the physical processes occurring near the surface of the Moon. The results of this work have shown that the relevant processes cannot be modeled with reasonable accuracy, mainly because we have no knowledge of many important parameters that actually determine the environment under study, and even those parameters that are known well can only be reproduced in terrestrial laboratory conditions with great difficulty. Due to many unsolved problems, studying the physical processes associated with the dynamics of lunar dust is currently difficult. Below, we list only the major problems, which we classify into several categories for convenience.

Clarifying the physical properties of regolith. This concerns, first and foremost, those properties of regolith that affect its photoemission and electrical conductivity. In

particular, the parameters of the regolith material such as the work function, quantum yield, influence of nanophase iron, dependence of electrical conductivity on temperature, and presence of water molecules in the upper regolith layers are still not sufficiently known. These parameters largely determine the strength of surface currents induced by external factors of the space environment, the magnitude of the electric charge of the surface, and the characteristics of the double sheets and parameters of the near-surface plasma. These characteristics of regolith can be obtained *in situ* or by laboratory analysis of regolith samples returned to Earth.

Problem of detachment of microparticles from the regolith surface. Currently, it is generally accepted that the most likely cause of the detachment of dust particles from the illuminated surface of atmosphereless celestial bodies is the electrostatic field. At least three forces act on a microparticle located on the regolith surface: the adhesion force, the force of gravity, which holds the particle on the surface, and the electrostatic force, which tries to tear the particle off the surface. There are several key open questions connected with this problem, primarily the assessment of the van der Waals adhesion force. This force and the force of gravity compete with each other, depending on the size, shape, and mass of a particle. Moreover, the adhesion force largely depends on the shape of the particle surfaces at the particle contact point, and therefore assessing the adhesion force in modeling is quite difficult. However, the key problem faced when solving the problem of particle detachment is to explain how the electric charge necessary for lifting off from the surface can accumulate on a dust grain still lying on the surface [6]. To date, there have been several studies devoted to this problem, e.g., [9, 152, 154, 155]. Various approaches were proposed there for solving the problem of the emergence of an electric field acting on a particle strong enough to overcome the forces holding the particle and to tear it off the surface. However, none of the existing models offers a self-consistent theory of such a physical process that would determine the magnitude of the flow of microparticles lifted off the surface, their mass, their speed, the magnitude of their electric charge, and the parameters of the near-surface electric field in the emerging plasma sheet. Today, the processes of detachment of dust particles from the surface and their dynamics appear more complex than previously thought, and the existing models require corrections. To explain the detachment of particles from the surface, we should apparently not only deal with the averaged description of the electric charge accumulation by near-surface dust particles but also take the random nature of these processes into account, given the discrete nature of the interaction of plasma particles and UV radiation with the regolith. A preliminary analysis shows that thermodynamic processes can also play a role in the detachment of submicron particles from the surface. Solving the problem of microparticle detachment from the regolith surface is important for constructing a self-consistent description of the dynamics of lunar regolith microparticles under the influence of solar radiation, solar plasma, and micrometeoroids.

Plasma–dust processes in terminator region at the boundary of light and shadow. The peculiarity of these regions is that the mechanisms for acquiring charge by the regolith change sharply at the boundary of light and shadow. As discussed above, on the illuminated side of the Moon, regolith is charged positively as a result of the photoelectric effect. On the night side or in the shadowed regions on the day side, the main role is played by the electrons of the incident flow of interplanetary plasma, and the surface is charged negatively. It was in the area of the terminator that LHG was observed, which gave impetus to studies of lunar dust. In the terminator region, where the zenith angle of the Sun approaches 90°, inhomogeneities of the regolith surface play an important role when sharp boundaries of light and shadow become strongly localized. Numerous studies have been devoted to the plasma–dust processes in the terminator region, but their nature remains an open problem. Another open question is about the possible effect of the observational selection of LHG in the terminator region and the conditions for observing levitating dust particles away from the boundary of light and shadow.

Processes in magnetic anomaly zones. The existence of local zones with an increased magnetic field on the surface of the Moon leads to peculiarities of the interaction of the incident plasma flow: mini-magnetospheres form in these zones, changing the conditions of the plasma–regolith interaction. These peculiarities were revealed by measurements from orbiting lunar probes, which only allowed studying these anomalies in the most general terms. For example, so-called lunar swirls are often associated with magnetic anomalies—regions with an increased albedo, where dust transport along the lunar surface is apparently increased. Of course, all these features observed from spacecraft in lunar orbit are of great interest and require further *in situ* studies of the dynamics of the plasma–dust exosphere in such zones.

Role of collateral dust. Among the unresolved problems, we mention the aggressive influence of collateral dust discovered during the American crewed Apollo mission, which we reviewed in Section 3. Although this problem is not associated with natural physical processes occurring on the Moon, the experience of the Apollo missions raised several important questions as to the influence of collateral lunar dust on the engineering systems of the landing vehicles and on the activities and health of astronauts on the Moon. Because several countries plan to expand Moon exploration, including with human participation, laboratory research is needed to study the influence of charged dust on materials and spacecraft systems and to develop methods for minimizing that influence [185]. Obviously, this 'practical' direction in studying the dynamics of lunar dust and creating tools for reducing its negative impact is also of great importance. In this regard, the problem arises of building theoretical models of the 'perturbed' state of the near-surface plasma–dust exosphere to simulate the appearance of collateral dust under anthropogenic influence.

These unsolved problems seem to be the most important ones in our opinion, but by no means exhaust all obstructions to understanding the physical processes occurring under the influence of external factors of outer space on the Moon and its regolith and to creating reliable models of such processes.

6. Instead of a conclusion

Finding a glow above the lunar horizon was the most unexpected discovery recorded by Soviet and American lunar landers in the very early stages of lunar exploration. The analysis of observational data led to assumptions that the observed glow is associated with the scattering of sunlight on microparticles levitating above the regolith surface at heights of several tens of centimeters. The six crewed missions to the lunar surface within NASA's Apollo program showed that

levitating particles exert an extremely negative effect on the engineering systems of lunar landing vehicles and on the activities and health of astronauts. Moreover, the experience of manned missions to the surface of the Moon has shown that anthropogenic activity has a much greater effect on the dynamics of lunar dust than natural processes occurring on the Moon. The 'dust problem' was quoted in astronauts' reports on their missions as the one that was the most complex and difficult to overcome in relation to human activities on the Moon. All the results collected by robotic and crewed expeditions showed that the study of the observed effects and processes associated with lunar dust has not only scientific but also practical significance in implementing further plans for the possible exploration of the Moon.

Results of pioneering studies of the Moon triggered the development of a new scientific area associated with so-called 'complex plasma,' in particular, dusty plasma, in which charged microparticles are present, as are ordinary ions. Due to the obvious difficulties of conducting full-scale experiments on the lunar surface, the main results were subsequently obtained by developing theoretical models and using laboratory modeling. At the same time, adequate modeling is difficult not only because of the need to create deep vacuum and low gravity conditions characteristic of the Moon but also, and primarily, because of the specific properties of the lunar dust microparticles themselves, which were formed in the process of high-speed impacts of micrometeorites and which are nonexistent in natural conditions on Earth. From a practical standpoint, such studies are important for assessing the impact of microparticles on various materials, service systems, mechanical components, and air-proof seals. A special and extremely important area is research into the impact of lunar dust on the activities of astronauts on the lunar surface and on human health.

An important component of laboratory modeling is the creation of analogues of lunar regolith, with characteristics close to the main parameters of lunar dust. The analogues are most often considered in terms of chemical, mineralogical, and granulometric compositions; in terms of specific features of dust particles, e.g., their extremely irregular shape, and the presence of nanophase iron on the surface of dust grains; and in terms of other characteristics specific to the Moon. Creating analogues of lunar regolith and its dust component is currently receiving considerable attention (see, e.g., [186]). As of 2021, the archive of existing regolith analogues (Planetary Simulant Database, https://simulantdb.com/index.php) includes 43 registered names of analogues created in the USA, China, and several other countries. Two of these analogues were used in preparation for the Chinese Chang'e-5 mission, which returned lunar regolith samples to Earth in 2021.

In Russia, laboratory experiments with dusty plasma were started under the leadership of Fortov [187] and continue being developed at the Joint Institute for High Temperatures of the Russian Academy of Sciences. Active work on modeling the dynamics of dust particles and simulating various conditions of outer space is underway at laboratory facilities of the Space Research Institute of the Russian Academy of Sciences, the Institute of Applied Physics of the Russian Academy of Sciences, and other organizations. These studies include experiments on the laboratory modeling not only of plasma–dust processes near the Moon but also of various phenomena occurring in other parts of the Solar System where dust particles play a significant and sometimes decisive role. Examples include planetary dust clouds, dust storms on Mars, cometary comas, 'dust lakes' on the Eros asteroid [188] and on the nucleus of the 67P Churyumov–Gerasimenko comet [189], radial spokes that periodically appear in the rings of Saturn [190], and many other phenomena in the Solar System and in the Universe as a whole. An important stage in the development of research in this area is the creation by the State Corporation Rosatom of a dedicated National Center for Physics and Mathematics (NCPM) aimed at experimental studies of astrophysical processes using laboratory modeling methods. One of the research fields of the NCPM will be the study of plasma–dust processes in the near-surface exosphere of the Moon.

Currently, the space agencies of several countries are drafting projects to study the Moon with orbital and landing spacecraft. The People's Republic of China has already successfully completed several expeditions in recent years, including the Chang'e-4 mission to land on the far side of the Moon and Chang'e-5 to return lunar regolith samples to Earth. In the coming years, the PRC plans to continue this program to explore the south polar region and build infrastructure there for studying natural resources and their possible utilization. India is also a player in Moon exploration. After two Indian orbital missions, Chandrayaan 1 and 2, Chandrayaan 3 was successfully completed in August 2023 by landing in the south polar region. Exploration of the Moon is also envisaged by Japan and the European Space Agency. In the USA, NASA, with the cooperation of more than 20 countries, is preparing an ambitious Artemis lunar exploration program with human participation.

In Russia, after an almost fifty-year break in lunar exploration via spacecraft, in accordance with the Federal Space Program, a series of lunar missions are planned to be launched in the coming years, carrying orbital and landing vehicles: Luna-25, Luna-26, Luna-27, and so on. The scientific program of these studies is aimed at continuing the exploration of the Moon at a new level of scientific research technology for space. The plan is that the landing vehicles will explore the vicinity of the South Pole of the Moon [191], where no spacecraft have yet landed. This area of the Moon has several characteristic and very important features, in particular:

(1) because the rotation axis of the Moon is nearly perpendicular to the ecliptic plane, the circumpolar regions of the Moon host places where the surface is almost constantly illuminated by the Sun (hence, almost an uninterrupted source of solar energy is ensured); in addition, almost constant radio communication with Earth can be ensured in such locations;

(2) according to measurements made by the Russian LEND instrument installed on the American LRO satellite orbiting the Moon, there are areas in the polar regions of the Moon with a reduced number of neutrons reflected as a result of their scattering in the regolith (the so-called neutron albedo), which is associated with the presence of water ice in subsurface regolith layers [192];

(3) the polar regions of the Moon, as regards the nature of changes in the zenith angle of the Sun, are very close to the terminator regions, where surface illumination conditions change sharply; this feature is extremely interesting for scientific research to elucidate the competing influence of solar illumination and solar wind plasma flows on the surface charging process and to study the dynamics of dust particles of the lunar regolith in such areas.

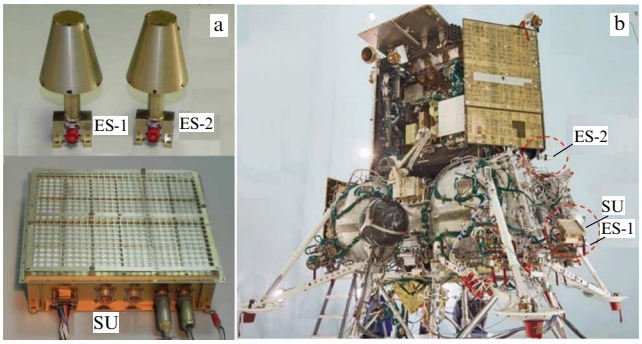

Figure 21. (a) Photos of LDM blocks. (b) Photo of Luna-25 spacecraft during tests. Locations of LDM blocks on the device are shown.

The scientific research program on the planned Luna-25 and Luna-27 landing vehicles includes (1) studies of the composition and of the physical, mechanical, and thermophysical properties of regolith in the surface layer to a depth of 1–2 m, assessment of the mass fraction of water ice in polar regolith, elucidation of the origin of water in polar regolith, and (2) studies of the properties and dynamics of the plasma, neutral, and dust components in the lunar polar exosphere.

The scientific equipment of the Luna-25 and Luna-27 landing vehicles includes the Lunar Dust Monitoring (LDM) device to detect lunar dust microparticles levitating above the regolith surface and determine the parameters of the near-surface plasma in which the dust particles move. Using this device on each lunar landing vehicle, the plan is to detect microparticles levitating above the lunar surface for a long time, assess their physical characteristics, and monitor the parameters of the near-surface plasma–dust environment (its concentration, temperature, and potential) [193, 194].

The LDM device on the Luna-25 spacecraft includes three elements: an impact sensor unit (SU) and two electrostatic sensors, ES-1 and ES-2. The sensitive elements of the SU block are 24 piezoelectric plates, the total aperture being $\sim 150 \times 150$ mm. Each ES block includes two sensors: a Langmuir probe and an inductive charge sensor. Figure 21 shows photographs of the LDM blocks and of the Luna-25 landing vehicle during tests, with the locations of the LDM blocks indicated.

The parameters of the lunar environment studied by the LDM instrument are very sensitive to the influence of the induced electric potential of the lander. Unfortunately, it was not possible to place a remote boom aboard the Luna-25 spacecraft for sensitive elements of the instrument blocks to be installed on it in order to eliminate the influence of the landing vehicle on the measurements. Therefore, using numerical modeling, the impact of the spacecraft on the environment was assessed in order to take this effect into account when analyzing the measurements to be performed [195].

The Luna-25 spacecraft was launched in August 2023, during the preparation of this paper. After the flight from Earth to the Moon, the spacecraft successfully entered a circular lunar orbit 100 km above the lunar surface. In this orbit, the LDM device was turned on to check its functionality. The results of switching the device on showed its operability and readiness to carry out measurements on the surface of the Moon. During the time ($\sim$ 45 min) when the LDM was turned on, 10 (out of 24) piezoelectric sensors of the device simultaneously registered an impact event. A preliminary analysis of this event led to the conclusion that such a response from the device could be caused by a micrometeoroid from the Perseid meteor shower that occurs annually in August.

During the further flight program — transferring the spacecraft into a prelanding elliptical orbit — a failure occurred in the control system, and the spacecraft was lost. The Roscosmos State Corporation has to resolve the issue: either make some adjustments to the previously planned lunar research program or go ahead with implementing it.

In accordance with the currently existing space program, the next vehicle to land on the lunar surface (after the Luna-25 spacecraft) should be Luna-27. The LDM device for it is built according to a scheme similar to that of the device installed on Luna-25. However, unlike Luna-25, the dust instrument for Luna-27 includes a remote boom on which sensitive impact sensors to detect microparticles above the regolith surface, Langmuir probes, and the inductive charge sensors of dust particles will be placed. This boom will significantly minimize the influence of the lander on the measurement results [195]. Langmuir probes are located on the boom at different heights from the surface to determine the vertical component of the near-surface electric field. Figure 22 shows a diagram of part of the landing vehicle body, the LDM blocks installed on it, and the boom in the deployed state.

The LDM device aboard Luna-27 will detect microparticles lifted off from the regolith surface under the influence of solar radiation and secondary particles knocked out in high-speed impacts of micrometeorites in the vicinity of the spacecraft landing site. The electrical sensors included in the device are designed to determine the main parameters of the near-surface plasma and electric fields in the near-surface exosphere and near the body of the lander (which will allow determining the influence of the spacecraft on plasma diagnostics). The sensors of the device will allow tracing

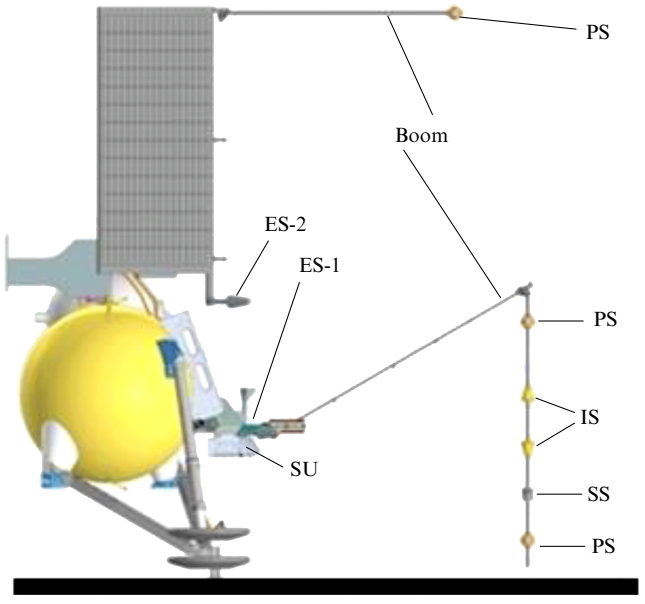

Figure 22. Portion of a diagram for the Luna-27 spacecraft. Location of LDM blocks is shown: SU (shock sensor), ES-1 and ES-2 (electrical sensors), and the boom with three probe sensors (PS, Langmuir probes), two induction sensors (IS), and shock sensors (SS, piezoceramic plates).

changes in the parameters of the near-surface plasma–dust environment, depending on local time and solar activity. The LDM operating program includes long-term measurements on the lunar surface. As the authors of the experiment hope, this will make it possible, on a time scale of one or several lunations (approximately 29 Earth days each), to compare the state of the plasma–dust exosphere perturbed by the burn of the spacecraft landing engines, i.e., in the presence of collateral dust, with the lunar environment conditions determined by natural external factors. The combination of all this data will allow obtaining important firsts — results that the participants in the planned research hope will offer insights into the mechanisms and features of the dynamics of lunar dust and near-surface plasma in the polar region of the Moon.

Acknowledgments. The study was carried out at the Space Research Institute of the Russian Academy of Sciences (project Planet) with the participation of the Institute of Metal Physics of the Ural Branch of the Russian Academy of Sciences (state assignment Electron, s.r. No. 122021000039-4) and supported by the State Atomic Energy Corporation Rosatom in the framework of the Experimental Laboratory Astrophysics and Geophysics research area in the Science Center for Physics and Mathematics.

References

1. Criswell D R, in *Photon and Particle Interactions with Surfaces in Space, Proc. of the 6th ESLAB Symp., Noordwijk, September 26–29, 1972* (Astrophysics and Space Science Library, Vol. 37, Ed. R J L Grard) (Dordrecht: D. Reidel Publ. Co., 1973) p. 545
2. Rennilson J J, Criswell D R *The Moon* **10** 121 (1974)
3. Berg O E, Wolf H, Rhee J, in *Interplanetary Dust and Zodiacal Light, Proc. of IAU Colloq. 31, Heidelberg, Germany, 10–13 June 1975* (Lecture Notes in Physics, Vol. 48, Eds H Elsaesser, H Fechtig) (Berlin: Springer, 1976) p. 233, https://doi.org/10.1007/3-540-07615-8_486
4. Carrier W D (III), Olhoeft G R, Mendell W et al., in *The Lunar Sourcebook, A User's Guide to the Moon* (Eds G H Heiken, D T Vaniman, B M French) (New York: Cambridge Univ. Press, 1991) p. 475
5. Colwell J E et al. *Rev. Geophys.* **45** RG2006/2007 (2007) https://doi.org/10.1029/2005RG000184
6. Hartzell C M, Scheeres D J *Planet. Space Sci.* **59** 1758 (2011)
7. Nitter T et al. *IEEE Trans. Plasma Sci.* **22** 159 (1994)
8. Borisov N, Mall U *J. Plasma Phys.* **67** 277 (2002)
9. Borisov N, Mall U *Planet. Space Sci.* **54** 572 (2006)
10. Poppe A, Horányi M *J. Geophys. Res.* **115** A08106 (2010)
11. Popel S I et al. *JETP Lett.* **99** 115 (2014); *Pis'ma Zh. Eksp. Teor. Fiz.* **99** 131 (2014)
12. Popel S I et al. *Planet. Space Sci.* **156** 71 (2018)
13. Sickafoose A A et al. *J. Geophys. Res.* **107** (A11) 1408 (2002) https://doi.org/10.1029/2002JA009347
14. Wang X, Horanyi M, Robertson S *J. Geophys. Res.* **114** A05103 (2009) https://doi.org/10.1029/2008JA013983
15. Dyal P, Parkin C W, Daily W D, in *Lunar Science Conf., 8th, Houston, Tex., March 14–18, 1977, Proc.* Vol. 1 (New York: Pergamon Press, 1977) p. 767
16. Olhoeft G R et al. *The Moon* **9** 79 (1974)
17. Gaier J R, Technical Memorandum NASA/TM-2005-213610 (Hanover, MD: NASA Center for Aerospace Information, 2005)
18. Linnarsson D et al. *Planet. Space Sci.* **74** 57 (2012)
19. Pieters C M, Noble S K *J. Geophys. Res. Planets* **121** 1865 (2016)
20. Kallio E et al. *Planet. Space Sci.* **166** 9 (2019)
21. O'Brien P O et al., in *50th Lunar and Planetary Science Conf., March 18–22, 2019, The Woodlands, Texas* (LPI Contrib., No. 2132) (Houston, TX: Lunar and Planetary Institute, 2019)
22. Grün E et al. *Icarus* **62** 244 (1985)
23. Melosh H J *Impact Cratering: a Geologic Process* (New York: Oxford Univ. Press, 1989); Translated into Russian: *Obrazovanie Udarnykh Kraterov: Geologicheskii Protsess* (Moscow: Mir, 1994)
24. Popel S I et al. *JETP Lett.* **103** 563 (2016); *Pis'ma Zh. Eksp. Teor. Fiz.* **103** 641 (2016)
25. Horányi M et al. *Nature* **522** 324 (2015)
26. Krüger H et al. *Icarus* **164** 1170 (2003)
27. Zook H A, in *Proc. of the Sixth Lunar Science Conf., Houston, Texas, March 17–21, 1975* (New York: Pergamon Press, 1975) p. 163
28. Grün E, Horanyi M, Sternovsky Z *Planet. Space Sci.* **59** 1672 (2011)
29. Brownlee D, Bucher W, Hodge P, in *Analysis of Surveyor 3 Material and Photographs Returned by Apollo 12* (NASA SP-284, Eds W F Carroll et al.) (Washington, DC: NASA, 1972) p. 143
30. Katzan C M, Edwards J L, NASA Contractor Report 4404 (Washington, DC: NASA, 1991)
31. Liu Y, Taylor L A *Planet. Space Sci.* **59** 1769 (2011)
32. Li D et al. *J. Geophys. Res. Planets* **124** 2168 (2019)
33. Zhang H et al. *Sci. China Tech. Sci.* **63** 520 (2020)
34. Golub' A P, Popel S I *Solar Syst. Res.* **55** 389 (2021); *Astron. Vestn.* **55** 393 (2021)
35. Haskin L, Warren P, in *The Lunar Sourcebook: A User's Guide to the Moon* (Eds G H Heiken, D T Vaniman, B M French) (Cambridge: Cambridge Univ. Press, 1991) p. 357
36. Walker R M *Annu. Rev. Earth Planet. Sci.* **3** 99 (1975)
37. Wurz P et al. *Icarus* **191** 486 (2007)
38. Tsurutani B T, Jones D E, Sibeck D G *Geophys. Res. Lett.* **11** 1066 (1984)
39. Tsurutani B T et al. *Geophys. Res. Lett.* **11** 1062 (1984)
40. Peterson W K, Shelley E G *J. Geophys. Res.* **89** 6729 (1984)
41. Frank L A *Space Sci. Rev.* **42** 211 (1985)
42. Rich F J, Reasoner D L, Burke W J *J. Geophys. Res.* **78** 8097 (1973)
43. Clay D R et al. *J. Geophys. Res.* **80** 1751 (1975)
44. Vaverka J et al. *Astrophys. J.* **825** 133 (2016)
45. Reedy R C, Arnold J R *J. Geophys. Res.* **77** 537 (1972)
46. Hendrix A R et al. *J. Geophys. Res.* **117** E12001 (2012)
47. Li X et al., in *Moon. Prospective Energy and Material Resources* (Ed. V Badescu) (Berlin: Springer, 2012) p. 347, https://doi.org/10.1007/978-3-642-27969-0_15
48. Jia B et al. *J. Geophys. Res. Planets* **126** e2021JE006934 (2021)
49. McKay D S, Ming D W *Development Soil Sci.* **19** 449 (1990)
50. Ivanov A V, Nazarov M A *Vestn. NPO im. S A Lavochkina* (4) 48 (2012)
51. Li C et al. *Natl. Sci. Rev.* **9** (2) nwab188 (2022)
52. Hapke B, Sato H *Icarus* **273** 75 (2016)
53. Hayne P O et al. *J. Geophys. Res. Planets* **122** 2371 (2017)
54. Leontovich A K, in *Lunnyi Grunt iz Morya Izobiliya* (Lunar Soil from the Sea of Plenty) (Exec. Ed. A P Vinogradov) (Moscow: Nauka, 1974) p. 563
55. Slyuta E N *Solar Syst. Res.* **48** 330 (2014); *Astron. Vestn.* **48** 358 (2016)
56. Agrell S O et al., in *Proc. of the Apollo 11 Lunar Science Conf., 5–8 January, 1970, Houston, TX* Vol. 1 *Mineralogy and Petrology* (Ed. A A Levinson) (New York: Pergamon Press, 1970) p. 93
57. Loftus D J et al. *Earth Moon Planets* **107** 95 (2010)
58. Taylor L A, Cirlen E H, in *ESR Dating and Dosimetry* (Eds M Ikeya, T Miki) (Tokyo: IONICS, 1985) p. 19
59. Keller L P, McKay D S *Science* **261** 1305 (1993)
60. Keller L P, McKay D S *Geochim. Cosmochim. Acta* **61** 2331 (1997)
61. Pieters C M et al. *Meteorit. Planet. Sci.* **35** 1101 (2000)
62. Taylor L A et al. *J. Geophys. Res. Planets* **106** 27985 (2001)
63. Morris R V, in *Lunar and Planetary Science Conf., 9th, Houston, Tex., March 13–17, 1978, Proc.* Vol. 2 (New York: Pergamon Press, 1978) p. 2287
64. Guo Z et al. *Geophys. Res. Lett.* **49** e2021GL097323 (2022)
65. Lu X et al. *Nat. Astron.* **7** 142 (2023)
66. McKay D S et al., in *The Lunar Sourcebook: A User's Guide to the Moon* (Eds G H Heiken, D T Vaniman, B M French) (New York: Cambridge Univ. Press, 1991) p. 285
67. Fa W et al., in *50th Lunar and Planetary Science Conf., 18–22 March, 2019, Woodlands, Texas* (LPI Contrib., No. 2132) (Houston, TX: Lunar and Planetary Institute, 2019)
68. Carrier W D (III) *The Moon* **6** 250 (1973)

69. Rode O D, Ivanov A V *Solar Syst. Res.* **18** 1 (1984); *Astron. Vestn.* **18** (1) 3 (1984)
70. Park J S et al., in *37th Lunar and Planetary Sciences Conf., March 13–17, 2006, League City, Texas* (New York: Pergamon Press, 2006) p. 2193
71. Kolmogorov A N *Dokl. Akad. Nauk SSSR* **31** 99 (1941)
72. Adushkin V V et al. *Dokl. Earth Sci.* **415** 820 (2007); *Dokl. Ross. Akad. Nauk* **415** 247 (2007)
73. Popel S I et al. *Solar Syst. Res.* **47** 419 (2013); *Astron. Vestn.* **47** 455 (2013)
74. Liu Y et al. *J. Aerospace Eng.* **21** 272 (2008)
75. Mahmood A et al., in *Proc. of the 5th Lunar and Planetary Sciences Conf.* (New York: Pergamon Press, 1974) p. 2347
76. Vaniman D et al., in *The Lunar Sourcebook*: *A User's Guide to the Moon* (Eds G H Heiken, D T Vaniman, B M French) (Cambridge: Cambridge Univ. Press, 1991) p. 27
77. Alvarez R "Lunar and terrestrial sample photoconductivity", in *Proc. of the Sixth Lunar Science Conf., Houston, Texas, March 17–21, 1975* Vol. 3 (New York: Pergamon Press, 1975) p. 3187
78. Halekas J S et al. *J. Geophys. Res. Planets* **106** 27841 (2001)
79. Lin R P et al. *Science* **281** 1480 (1998)
80. Vyshlov A S, Savich N A *Cosmic Res.* **16** 450 (1979); *Kosmicheskie Issled.* **16** 551 (1978)
81. Vasil'ev M B et al. *Cosmic Res.* **12** 102 (1974); *Kosmicheskie Issled.* **12** 115 (1974)
82. Vyshlov A S, in *Space Research XVI*; *Proc. of the Open Meetings of Working Groups on Physical Sciences, May 29 – June 7, 1975, and Symp. and Workshop on Results from Coordinated Upper Atmosphere Measurement Programs, Varna, Bulgaria, May 29–31, 1975* (Berlin: Akademie-Verlag GmbH, 1976) p. 945
83. Imamura T et al. *J. Geophys. Res.* **117** A06303 (2012)
84. Stern S A *Rev. Geophys.* **37** 453 (1999)
85. Stubbs T J et al. *Planet. Space Sci.* **59** 1659 (2011)
86. Reasoner D L, Burke W J, in *Photon and Particle Interactions with Surfaces in Space. Proc. of the 6th ESLAB Symp., Noordwijk, September 26–29, 1972* (Astrophysics and Space Science Library, Vol. 37, Ed. R J L Grard) (Dordrecht: Reidel, 1973) p. 369
87. Vondrak R R, in *The Second Conf. on Lunar Bases and Space Activities of the 21st Century* (NASA Conf. Publ. 3166, Vol. 1, Ed. W W Mendell) (Washington, DC: NASA, 1988) p. 337
88. Hodges R R, Hoffman J H, in *Proc. of the Sixth Lunar Science Conf., Houston, Texas, March 17–21, 1975* (New York: Pergamon Press, 1975) p. 3039
89. Hoffman J H, Hodges R R (Jr.), Evans D E, in *Proc. of the 4th Lunar and Planetary Sciences Conf.* (New York: Pergamon Press, 1973) p. 2875
90. Vondrak R R *Nature* **248** 657 (1974)
91. Potter A E, Morgan T H *Science* **241** 675 (1988)
92. Tyler A L et al. *Geophys. Res. Lett.* **15** 1141 (1988)
93. Popel S I et al. *JETP Lett.* **105** 635 (2017); *Pis'ma Zh. Eksp. Teor. Fiz.* **105** 594 (2017)
94. Zel'dovich Ya B, Raizer Yu P *Physics of Shock Waves and High-Temperature Hydrodynamic Phenomena* (Mineola, NY: Dover Publ., 2002); Translated from Russian: *Fizika Udarnykh Voln i Vysokotemperaturnykh Gidrodinamicheskikh Yavlenii* (Moscow: Nauka, 1966) p. 458
95. Al'pert Ya L, Gurevich A V, Pitaevskii L P *Sov. Phys. Usp.* **6** 13 (1963); *Usp. Fiz. Nauk* **79** 23 (1963)
96. Lue C et al. *J. Geophys. Res. Space Phys.* **123** 5289 (2018)
97. Feuerbacher B et al. *Geochim. Cosmochim. Acta* **3** 2655 (1972)
98. Willis R F, in *Photon and Particle Interactions with Surfaces in Space, Proc. of the 6th ESLAB Symp., Noordwijk, September 26–29, 1972* (Astrophysics and Space Science Library, Vol. 37, Ed. R J L Grard) (Dordrecht: Reidel, 1973) p. 389
99. Walbridge E *J. Geophys. Res.* **78** 3668 (1973)
100. Sternovsky Z et al. *J. Geophys. Res.* **113** A10104 (2008)
101. Vondrak R R, private communication (2012)
102. Popel S I et al. *J. Plasma Phys.* **79** 1071 (2013)
103. Popel S I, Golub' A, Zelenyi L *Eur. Phys. J. D* **68** 245 (2014)
104. Chamberlin P C, Woods T N, Eparvier F G *Space Weather* **5** S07005 (2007)
105. Nitter T, Havnes O, Melandsø F *J. Geophys. Res.* **103** 6605 (1998)
106. Lisin E A et al. *JETP Lett.* **98** 664 (2013); *Pis'ma Zh. Eksp. Teor. Fiz.* **98** 755 (2013)
107. Mishra S K *Phys. Plasmas* **27** 082906 (2020)
108. Fowler R H *Statistical Mechanics*: *The Theory of the Properties of Matter in Equilibrium* (London: Cambridge Univ. Press, 1955)
109. Sodha M S, Dixit A, Srivastava S *Appl. Phys. Lett.* **94** 251501 (2009)
110. Bhardwaj A et al. *Geosci. Lett.* **2** 10 (2015)
111. McComas D J et al. *Geophys. Res. Lett.* **36** L12104 (2009)
112. Wieser M et al. *Planet. Space Sci.* **57** 2132 (2009)
113. Saito Y et al. *Geophys. Res. Lett.* **35** L24205 (2008)
114. Katz I et al., Technical Report, NASA CR-135256, SSS-R-77-3367 (Washington, DC: National Technical Information Service, 1977)
115. Alnussirat S T et al. *Nucl. Instrum. Meth. Phys. Res. B* **420** 33 (2018)
116. Sarantos M et al. *Geophys. Res. Lett.* **35** L04105 (2008)
117. McCracken G M *Rep. Prog. Phys.* **38** 241 (1975)
118. McGrath M A, Johnson R E, Lanzerotti L J *Nature* **323** 694 (1986)
119. Yokota S, Saito Y *Earth Planets Space* **57** (4) 281 (2005)
120. Baragiola R A *Nucl. Instrum. Meth. Phys. Res. B* **88** 35 (1994)
121. Cladis J B, Francis W E, Vondrak R R *J. Geophys. Res.* **99** (A1) 53 (1994)
122. Manka R H, in *Photon and Particle Interactions with Surfaces in Space, Proc. of the 6th ESLAB Symp., Noordwijk, September 26–29, 1972* (Astrophysics and Space Science Library, Ed. R J L Grard) (Dordrecht: D. Reidel Publ. Co., 1973) p. 347, https://doi.org/10.1007/978-94-010-2647-5_22
123. Freeman J W, Ibrahim M *The Moon* **8** 103 (1975)
124. Goldstein B E *J. Geophys. Res.* **79** (1) 23 (1974)
125. De B R, Criswell D R *J. Geophys. Res.* **82** 999 (1977)
126. Criswell D R, De B R *J. Geophys. Res.* **82** 1005 (1977)
127. Halekas J S et al. *Geophys. Res. Lett.* **29** 1435 (2002)
128. Halekas J S, Lin R P, Mitchell D L *Geophys. Res. Lett.* **32** L09102 (2005)
129. Halekas J S et al. *J. Geophys. Res.* **113** A09102 (2008)
130. Severny A B, Terez E I, Zvereva A M *The Moon* **14** 123 (1975)
131. Benson J *J. Geophys. Res.* **82** 1917 (1977)
132. Farrell W M et al. *Geophys. Res. Lett.* **35** L05105 (2008)
133. Popel S I, Zelenyi L M, Atamaniuk B *Plasma Phys. Rep.* **42** 543 (2016); *Fiz. Plazmy* **42** 555 (2016)
134. Anuar A K *J. Phys. Conf. Ser.* **852** 012001 (2017)
135. Order N C et al. *Adv. Space Res.* **62** 896 (2018)
136. Berezhnoy A A et al. *Planet. Space Sci.* **177** 104689 (2019)
137. Li D et al. *Geophys. Res. Lett.* **47** e2020GL089433 (2020)
138. Popel S I, Zelenyi L M, Atamaniuk B *Phys. Plasmas* **22** 123701 (2015)
139. Farrell W M et al. *Geophys. Res. Lett.* **34** L14201 (2007)
140. Farrell W M et al. *J. Geophys. Res.* **115** E03004 (2010)
141. Poppe A R et al. *Icarus* **221** 135 (2012)
142. McCoy J E, Criswell D R, in *Lunar Science Conf., 5th, Houston, Tex., March 18–22, 1974, Proc.* (New York: Pergamon Press, 1974) p. 2991
143. Zook H A, Potter A E, Cooper B L "The Lunar Dust Exosphere and Clementine Lunar Horizon Glow", in *The Lunar and Planetary Science Conf.* Vol. 26 (Houston, TX: Lunar and Planetary Institute, 1995) p. 1577
144. Borisov N, Zakharov A *Planet. Space Sci.* **117** 295 (2015)
145. Hinteregger H E *Space Sci. Rev.* **4** 461 (1965)
146. Ivanov-Kholodnyi G S, Firsov V V *Geomagn. Aeronomy* **14** 331 (1975); *Geomagn. Aeronom.* **14** 393 (1974)
147. Kolesnikov E K, Manuilov A S *Sov. Astron.* **26** 602 (1982); *Astron. Zh.* **59** 996 (1982)
148. Izvekova Yu N, Morozova T I, Popel S I *IEEE Trans. Plasma Sci.* **46** 731 (2017)
149. Popel S I, Morozova T I *Plasma Phys. Rep.* **43** 566 (2017); *Fiz. Plazmy* **43** 474 (2017)
150. Horányi M et al., in *Lunar Dust 2020* (LPI Contrib., No. 2141) (2020)
151. Singer S F, Walker E H *Icarus* **1** (2) 112 (1962)
152. Flanagan T M, Goree J *Phys. Plasmas* **13** 123504 (2006)
153. Sheridan T E, Hayes A *Appl. Phys. Lett.* **98** 091501 (2011)
154. Wang X et al. *Geophys. Res. Lett.* **43** 6103 (2016)
155. Rosenfeld E V, Zakharov A V *Icarus* **338** 113538 (2020)
156. Hamaker H C *Physica* **4** 1058 (1937)
157. Li Q, Rudolph V, Peukert W *Powder Technol.* **161** 248 (2006)

158. Walch B, Horanyi M, Robertson S *IEEE Trans. Plasma Sci.* **22** (2) 97 (1994)
159. Sheridan T E et al. *J. Geophys. Res.* **97** 2935 (1992)
160. Sheridan T E *J. Appl. Phys.* **113** 143304 (2013)
161. Rosenfeld E V, Zakharov A V, Djakin V V *Langmuir* **38** 9382 (2022)
162. Hasani M et al. *J. Phys. D* **56** 025202 (2023)
163. Karlstrom K, Jonsson B, Preprint Lund Univ. (Lund: Lund Univ., 2013)
164. Rosenfeld E V et al. *Adv. Space Res.* **58** 560 (2016)
165. Dyal P et al. *Rev. Geophys.* **12** 568 (1974)
166. Mitchell D L et al. *Icarus* **194** 401 (2008)
167. Tsunakawa H et al. *Space Sci. Rev.* **154** 219 (2010)
168. Halekas J S et al. *Planet. Space Sci.* **56** 941 (2008)
169. Futaana Y et al. *Planet. Space Sci.* **54** 32 (2006)
170. Wieser M et al. *Geophys. Res. Lett.* **37** L05103 (2010)
171. Bamford R A et al. *Phys. Rev. Lett.* **109** 081101 (2012)
172. Vaisberg O L et al., in *Plazmennaya Geliogeofizika* (Plasma Heliogeophysics) Vol. 1 (Eds L M Zelenyi, I S Veselovskii) (Moscow: Fizmatlit, 2008) p. 378
173. Harnett E M, Winglee R M *J. Geophys. Res.* **107** 1421 (2002)
174. Blewett D T et al. *J. Geophys. Res.* **116** E02002 (2011)
175. Kramer G Y et al. *J. Geophys. Res.* **116** E00G04 (2011)
176. Garrick-Bethell I, Head J W (III), Pieters C M *Icarus* **212** 480 (2011)
177. Harada Y *Interactions of Earth's Magnetotail Plasma with the Surface, Plasma, and Magnetic Anomalies of the Moon* (Springer Theses) (Tokyo: Springer, 2015) Doctoral Thesis, https://doi.org/10.1007/978-4-431-55084-6
178. Popel S I et al. *Phys. Plasmas* **29** 013701 (2022)
179. Gaier J R, in *The Impact of Lunar Dust on Human Exploration, held 11–13 February, 2020, Houston, Texas* (LPI Contrib. No. 2141) (Houston, TX: LPI, 2020) id. 5002
180. Murphy T W (Jr.) et al. *Icarus* **211** 1103 (2011)
181. Carroll W F, Blair P M (Jr.), in *Analysis of Surveyor 3 Material and Photographs Returned by Apollo 12* (NASA SP–284) (Washington, DC: NASA, 1972) p. 23
182. Milwitzky B (Ed.) "Analysis of Surveyor 3 material and photographs returned by Apollo 12", NASA Report 1972 (Washington, DC: NASA, 1972)
183. O'Brien B J, Gaier J R, Indicative Basic Issues about Lunar Dust in the Lunar Environment. White Paper for the National Academies Planetary Sciences Decadal Survey (2009)
184. Christoffersen R et al., NASA/TP 2009-214786 (Hanover, MD: NASA Center for AeroSpace Information, 2009)
185. Afshar-Mohajer N et al. *Adv. Space Res.* **56** 1222 (2015)
186. Slyuta E N et al. *Acta Astronautica* **187** 447 (2021)
187. Fortov V E et al. *Phys. Lett. A* **267** 179 (2000)
188. Robinson M et al. *Nature* **413** 396 (2001)
189. Thomas N et al. *Science* **347** aaa0440 (2015)
190. Smith B A et al. *Science* **215** 504 (1982)
191. Zelenyi L M et al., in *Vklad Akademicheskoi Nauki v Razvitie Kosmicheskoi Otrasli. Nauchnye Sessii Obshchego Sobraniya Chlenov RAN i Obshchikh Sobranii Otdelenii RAN, Aprel', 2021 g.* (Contribution of Academic Science to the Development of the Space Industry. Scientific Sessions of the General Meeting of Members of the Russian Academy of Sciences and General Meetings of Branches of the Russian Academy of Sciences, April, 2021) (Eds A M Sergeev, V G Bondur, A A Makosko) (Moscow: RAN, 2022) p. 157
192. Mitrofanov I G et al. *Science* **330** 483 (2010)
193. Kuznetsov I A et al. *Solar Syst. Res.* **51** 611 (2017); Translated from Russian: *Vestn. NPO im. S A Lavochkina* (4) 20 (2016)
194. Zakharov A V et al. *Solar Syst. Res.* **55** 576 (2021); *Astron. Vestn.* **55** 589 (2021)
195. Kuznetsov I A et al. *Planet. Space Sci.* **156** 62 (2018)